

Effects of Pore Structure on Mixing in
Stable, Single-Phase Miscible Displacements

by

Robert Michael Specter

Submitted to the Faculty of the Graduate School of the
New Mexico Institute of Mining and Technology
in Partial Fulfillment of the Requirements for the Degree of
Master of Science in Geology

July 1984

N.M.I.M.T.
LIBRARY
SOCORRO, N.M.

EFFECTS OF PORE STRUCTURE ON MIXING IN
STABLE, SINGLE-PHASE MISCIBLE DISPLACEMENTS

ABSTRACT

Phase compositions strongly influence the ability of CO₂ to extract hydrocarbons during a CO₂ flood. Fluid compositions which occur are the result of mixing of CO₂, oil and water as they flow through porous reservoir rock. Mixing is influenced by diffusion and dispersion within pore networks in the rocks. Quantifiable features of pore structure which seem to influence mixing most are pore size and pore connectivity. Pore shape, coordination number, aspect ratio, flowpath tortuosity and permeability are also factors which must influence displacement results, but do so in less obvious and quantifiable ways. To examine the relationship between pore structure and mixing, four carbonate and three sandstone cores were examined in thin section and with electron microscopy. Complete petrographic analysis was performed on each sample, including determination of pore size distributions and connectivity patterns. Stable, single-phase miscible displacements performed in the cores were interpreted using a mixing model proposed by Coats and Smith (1964). Pore structure data are related to Coats-Smith parameters to determine the effects of pore structure on mixing phenomena. Average mixing behavior on the scale of short laboratory cores is qualitatively consistent with observations of pore structure in thin section. Small-scale heterogeneity of pore structure is responsible for mixing effects which result in early breakthrough of the displacing fluid and a flowing fraction less than one. A wide distribution of pore sizes is necessary but not in itself sufficient to produce a low flowing fraction. Also required are pore connections which result in the generation of preferential flow paths. Dispersion coefficients are significantly higher for the carbonates than for the sandstones. Large dispersion coefficients are associated with wide pore size distributions.

This thesis is accepted on behalf of the faculty
of the Institute by the following committee:



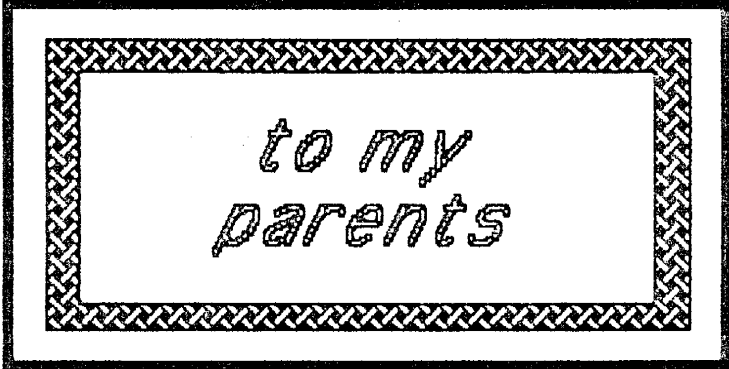
Adviser





July 31, 1984

Date



*to my
parents*

TABLE OF CONTENTS

Acknowledgements	v
List of Figures	vi
List of Tables	viii
Key to Symbols	ix
1. Background, Previous Work and Purpose	1.1
2. Mixing During Single-Phase Miscible Displacements in Reservoir Cores	2.1
Single-Phase Displacements	2.1
Mixing in Rocks	2.5
3. Sample Examination Methods	3.1
Whole Core Analysis	3.1
Thin Section Preparation	3.1
Thin Section Petrography	3.2
SEM and EDX Analysis	3.5
X-ray Diffraction of Clay Minerals	3.5
Flowpath Vector Analysis	3.6
Spatial Distribution of Pores	3.8
Single-Phase Displacements	3.11
4. Petrologic Elements Related to Porosity and Permeability Development	4.1
Pore Development in the Sandstone Samples ...	4.1
Petrology and Pore Structure of the Sandstone Cores	4.3
Pore Development in the Carbonate Samples ...	4.16
Petrology and Pore Structure of the Carbonate Cores	4.17
5. Relation of Pore Structure Observations to Displacement Results	5.1
Sandstone Cores	5.1
Carbonate Cores	5.8
Summary of Results	5.17
Discussion of Methodology	5.18
Questions of Scale	5.23
Future Work	5.26
6. Summary and Conclusions	6.1
References Cited	R.1
Appendix A: Petrographic Data	A.1

ACKNOWLEDGEMENTS

I am indebted to Dr. Franklin M. Orr, Jr. for supervising my research program and for providing enthusiastic support of this work. Working with Lynn has shown me that the traditional Geologist vs. Engineer conflict may be overcome when each keeps an open mind and ideas are exchanged.

Dr. David B. Johnson acted as my major advisor and Dr. John R. MacMillan also served on my thesis committee. Both of them assisted in planning the research program, interpreting data and editing this manuscript. Their efforts are greatly appreciated.

Financial support for this work was provided by the New Mexico Petroleum Recovery Research Center, the New Mexico Energy Research and Development Institute, the United States Department of Energy, and a consortium of corporations including the Abu Dhabi Reservoir Research Foundation, American Cyanamid, AMOCO Foundation, ARCO Oil & Gas, CONOCO, Marathon, Mobil, Shell Development, SOHIO, Sun Exploration & Development, and TENNECO.

Dr. Robert E. Bretz, Stephen L. Welch, Mary L. Graham and Michael P. Mayer collected the miscible displacement data.

Heidi L. Miller edited the manuscript. Janet E. Golding typed tables and figure captions, and M. David McKallip made available his MacIntosh computer and graphics software.

My parents have been very supportive and very, very patient.

LIST OF FIGURES

- Figure 2.1 Typical Effluent Composition Profile
for a Homogeneous Porous Medium
- Figure 2.2 Idealized Pore Systems
- Figure 3.1 "Union Jack" Configuration
- Figure 3.2 Flowpath Vector Analysis Method
- Figure 3.3 Method of Determining the Spatial
Distribution of Pores
- Figure 3.4 Typical Spatial Pore Distributions
- Figure 4.1 Grain Contacts in Sandstones
- Figure 4.2 Secondary Porosity in Sandstones
- Figure 4.3 Photomicrograph of B1
- Figure 4.4 Distribution of Pore Body Sizes for B1
- Figure 4.5 Spatial Distribution of Pores in B1
- Figure 4.6 Photomicrograph of F2
- Figure 4.7 Distribution of Pore Body Sizes for F2
- Figure 4.8 Spatial Distribution of Pores in F2
- Figure 4.9 Photomicrograph of R1
- Figure 4.10 Distribution of Pore Body Sizes for R1
- Figure 4.11 Spatial Distribution of Pores in R1
- Figure 4.12 Photomicrograph of WW2
- Figure 4.13 Distribution of Pore Body Sizes for WW2
- Figure 4.14 Spatial Distribution of Pores in WW2
- Figure 4.15 Distribution of Pore Body Sizes for H1
- Figure 4.16 Photomicrograph of H1
- Figure 4.17 Photomicrograph of H1
- Figure 4.18 Spatial Distribution of Pores in H1

LIST OF FIGURES - Continued

- Figure 4.19 Photomicrograph of SAO
- Figure 4.20 Distribution of Pore Body Sizes for SAO
- Figure 4.21 Photomicrograph of SAO
- Figure 4.22 Spatial Distribution of Pores in SAO
- Figure 4.23 Photomicrograph of M1
- Figure 4.24 Photomicrograph of M1
- Figure 4.25 Distribution of Pore Body Sizes for
the Lower 84% of Porosity in M1
- Figure 4.26 Distribution of Pore Body Sizes for M1
- Figure 4.27 Photomicrograph of M1
- Figure 4.28 Spatial Distribution of Pores in M1
- Figure 5.1 Effluent Composition Curve for B1
- Figure 5.2 " " " " F2
- Figure 5.3 " " " " R1
- Figure 5.4 " " " " WW2
- Figure 5.5 " " " " SAO
- Figure 5.6 " " " " H1
- Figure 5.7 " " " " M1
- Figure 5.8 Relation Between Flowpath Vector
Strength and Dispersion
- Figure 5.9 Relation Between Flowpath Vector
Strength and Flowing Fraction

LIST OF TABLES

Table 3.1	Mean Pore Sizes Used in Construction of Spatial Pore Distributions
Table 5.1	Summary of Miscible Displacement Results
Table 5.2	Summary of Pore Space Data
Table 5.3	Summary of Flowpath Vector Analysis Data
Table A.1	Summary of Core Properties
Table A.2a	Petrographic Data for Sandstone Cores
Table A.2b	Petrographic Data for Carbonate Cores
Table A.3	Identification of Clay Minerals by X-ray Diffraction

KEY TO SYMBOLS

- a - Damkhöler number; a dimensionless mass transfer group
(KL/u)
- c - concentration in the flowing stream
- c^* - concentration in the stagnant pore volume
- D - dispersion coefficient (cm^2/sec)
- f - flowing fraction
- K - mass transfer coefficient (sec^{-1})
- k_a - permeability to air
- L - length of displacement medium
- Pe - Peclet number; dimensionless indicator of dispersion
(uL/D)
- \bar{r}_f - magnitude of mean flowpath vector
- u - average interstitial flow velocity (ft/day or cm/sec)
- V_i - volume of fluid injected
- V_o - volume of effluent fluid
- β - peak height of effluent composition curve,
in pore volumes
- τ - dimensionless time scale, in pore volumes
- $\bar{\theta}$ - mean direction of flow, referenced from zero degrees

CHAPTER 1

BACKGROUND, PREVIOUS WORK AND PURPOSE

Phase compositions which occur in CO₂ displacements are the result of mixing of CO₂, oil and water as they flow through porous reservoir rock. Chemical engineers have created a substantial body of literature which is concerned with the phase behavior of fluids under a variety of physical and chemical conditions. Likewise, geologists have long been examining characteristics of pore structure, not only for determining levels of petroleum production from established fields but also in developing predictive exploration models for undiscovered resources. An increasing number of workers are concentrating on bridging the gap between the two disciplines, because it is apparent that an understanding of how fluids move, mix and interact within a reservoir requires such interdisciplinary study.

Displacement of oil by CO₂ in reservoirs is a complicated process both from the phase behavior and reservoir pore structure points of view (Spence and Watkins, 1980, Gardner et al., 1981, Orr and Taber, 1984). Phase compositions strongly influence the ability of CO₂ to extract hydrocarbons in a CO₂ flood, and hence they determine the efficiency of a flood. Fluid compositions that occur are the result of mixing within the pore structure of the reservoir; mixing is influenced by diffusion and dispersion.

Though much work has been done to describe flow behavior in displacements, few studies have been undertaken to examine the effects of pore structure on mixing in natural porous media. Mathematical modeling of displacements is a convenient method of predicting flow behavior. Many investigators have attempted to model the mixing that occurs as fluids flow. Taylor (1953) described the mixing that occurs by simple radial diffusion across a velocity profile in a capillary tube. Perkins and Johnston (1963) wrote a comprehensive discussion of diffusion and dispersion in porous media. They examined the model of a porous medium as a network of flow chambers with random size and flow conductivity, connected by openings of smaller size; flow behavior in this uniform system could be modeled by simple dispersion alone. Further, Perkins and Johnston discussed factors affecting mixing such as particle size distribution, particle shape and packing heterogeneities in unconsolidated grain packs.

To describe flow in heterogeneous pore systems, Deans (1963) devised a two-parameter flow model which divides the pore system into two components: the flowing stream in which mixing does not occur, and stagnant pores in which fluids are exchanged with those in the flowing stream by diffusion. Coats and Smith (1964) refined Deans' model into a three-parameter model which assumes dispersion in the flowing stream and diffusion from the stagnant pore volume. The Coats-Smith model is discussed further in Chapter 2; it

is this model of flow which is used for the determination of the displacement results examined in this study. Yellig and Baker (1980) considered the physical significance of the Coats-Smith model and determined that the parameters do not individually have physical significance. They suggested use of an "effective dispersion coefficient" which incorporates the three Coats-Smith parameters into one term. Yellig and Baker further pondered the difficulty of scaling up laboratory displacements to the reservoir level. They showed that as system length increases, mixing in heterogeneous media can be described by a simple dispersion model which features the effective dispersion coefficient.

The present study is concerned with mixing behavior in very complicated porous media, specifically, natural reservoir rocks. Due to the complexity of rock pore systems, it is desirable to begin with simple fluids and develop an understanding of how they mix before advancing to more complicated multiphase systems. To this end, this thesis examines the composition and pore system character of four carbonate and three sandstone cores. Data describing pore structure are related to results of single-phase, unit-mobility-ratio miscible displacements in the cores.

While a number of efforts have been made to examine complex fluids in very simple porous media (Simon and Kelsey, 1971, 1972, Morrow, 1979, Orr, Silva and Lien, 1983, and others), very few workers have previously attempted to relate mixing parameters to pore structure in reservoir

cores. Spence and Watkins (1980) commented on the relation between low flowing fractions and wide pore size distributions.

Related geological studies of reservoir cores have addressed the classification of porosity and permeability, development and destruction of pores within strata, and morphology of pore structure in rocks. For example, a method of classifying pore space in carbonates, devised by Archie (1952), is purely descriptive and is designed to infer information on pore structures too small to be observed under the petrographic microscope. Choquette and Pray (1970) developed a morphogenic classification of pore space for geologic facies interpretation. Lucia (1983) classified pore space in carbonates according to size and inter-connectivity.

Murray (1960) discussed formation of porosity in carbonate rocks due to both depositional and diagenetic processes, specifically the formation of dolomite. Longman (1980) related climate to preservation of both primary and secondary porosity in carbonates. Pittman (1971) examined the factors which influence microporosity development in carbonate rocks. Donath et al. (1980) experimentally produced secondary porosity in a limestone core by pressuring the core while injecting an acidic solution. Cussey and Friedman (1977) related pressure solution to porosity preservation in ooid reservoirs of France. Enos and Sawatsky (1981) related porosity and permeability to

particle size and degree of cementation in carbonate sediments. Wardlaw (1980) examined the effects of pore structure on multiphase displacement efficiency, both in rocks and in glass micromodels. No previous studies have been done which relate mixing of even the simplest fluids to pore structure in cores.

The program of research described here was designed to investigate the following questions.

1. What is the nature of the relationship between pore structure and fluid mixing?
2. Which characteristics of reservoir rocks affect displacement efficiency?
3. Can the Coats-Smith model parameters be related to pore structure in rocks?

Chapter 2 describes the principles which underlie displacement theory, reviews the Coats-Smith model, examines the petrophysical properties of pore systems and discusses their influence on mixing. In Chapter 3, a description of the methods used to analyze the sample cores is presented along with an explanation of data manipulation. Chapter 4 discusses the geological processes responsible for pore system development in the studied samples, and their resulting pore structure. Idealized physical models of pore systems and predicted flow behavior of fluids in them are also discussed. A discussion of results is given in Chapter 5, which also includes comparison of displacement results with pore structure of each studied sample. Conclusions of this work are presented in Chapter 6. Petrographic and other core data are found in Appendix A.

CHAPTER 2

MIXING DURING SINGLE-PHASE MISCIBLE DISPLACEMENTS IN RESERVOIR CORES

Single-Phase Displacements

The following discussion of single-phase displacements is condensed from Orr and Taber (1984). In miscible displacements, a transition zone develops between the displaced and displacing fluids. As the displacement progresses, the transition zone grows due to molecular diffusion, to mixing caused by variable flow velocities within individual pores (Taylor, 1953) and to mixing which results from non-uniform flowpath length caused by pore-scale heterogeneities in the porous medium.

In miscible displacement experiments, the composition profile cannot be easily measured at a fixed time. Instead, the compositions of fluids passing a fixed point, the core outlet, are measured. In a typical experiment, a core is saturated with one fluid, then a pulse of a second (displacing) fluid is injected. A plot of effluent concentrations against time (Figure 2.1) for a displacement in a homogeneous medium will be slightly asymmetric since the transition zone continues to expand during the time period in which it is produced.

A simple diffusion model is used to show the symmetric expansion of the transition zone. The model uses

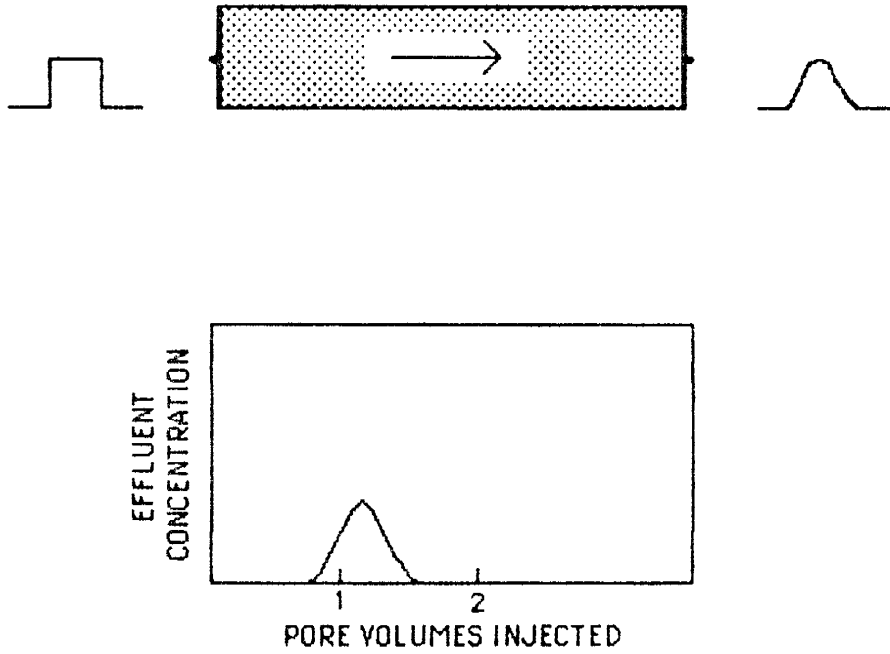


Fig. 2.1 Typical Effluent Composition Profile for a Homogeneous Porous Medium

one dimensionless parameter, the Peclet number (Pe). The Peclet number is related to the flow velocity, dispersion coefficient and length of the mixing chamber as defined in Equation 2.1.

$$\frac{\partial c}{\partial \tau} + \frac{\partial c}{\partial \xi} - \frac{1}{Pe} \frac{\partial^2 c}{\partial \xi^2} = 0 \quad (2.1)$$

$$Pe = \frac{uL}{D}$$

where: c = concentration in the flowing stream
 ξ = dimensionless length scale
 τ = dimensionless time scale in pore volumes
 Pe = Peclet number
 u = velocity of interstitial flow
 D = dispersion coefficient (core-scale)
 or diffusion coefficient (pore-scale)
 L = length of mixing chamber

The higher the Peclet number, the lower the effect of dispersion in the displacement process. The length of the "mixing chamber" previously referred to is a critical factor when considering Peclet values. When L is scaled to the order of a pore diameter, a "microscopic" Peclet number results, which describes the role of diffusion at the pore level. When L is considered to be the length of the displacement core, a "macroscopic" Peclet number which describes dispersion over the length of the core results.

In many displacements, observed effluent composition profiles are more asymmetric than can be explained by transition zone growth alone. Deans (1963) and Coats and Smith (1964) proposed models to account for the asymmetry. Both models hypothesized that some portion of the porous

medium might be stagnant, so that fluid present in such "dead-end pore volume" (DEPV) would be recovered only by mass transfer into the flowing stream. Deans' model considered mass transfer from DEPV by means of a "flowing fraction" parameter and a mass transfer coefficient. Flowing fraction (f) is defined by Deans (1963) as the fraction of total pore volume in a porous medium which is occupied by mobile fluid. Deans' model has the form

$$f \frac{\partial c}{\partial \tau} + (1-f) \frac{\partial c^*}{\partial \tau} + \frac{\partial c}{\partial \xi} = 0 \quad (2.2)$$

$$(1-f) \frac{\partial c^*}{\partial \tau} = a(c-c^*)$$

where: f = flowing fraction
 c^* = concentration in DEPV
 a = dimensionless mass transfer coefficient
(Damkohler number, KL/u)
 K = mass transfer coefficient (sec^{-1})

The model proposed by Coats and Smith, called the differential capacitance model, accounted for mass transfer from DEPV as well as longitudinal dispersion. Their model has the form

$$f \frac{\partial c}{\partial \tau} + (1-f) \frac{\partial c^*}{\partial \tau} + \frac{\partial c}{\partial \xi} - \frac{1}{Pe} \frac{\partial^2 c}{\partial \xi^2} = 0 \quad \begin{array}{l} 0 \leq \xi \leq 1 \\ \tau > 0 \end{array} \quad (2.3)$$

$$(1-f) \frac{\partial c^*}{\partial \tau} = a(c-c^*)$$

By using the flowing fraction (f), the Peclet number (Pe)

and the mass transfer group (α) to describe flow, the Coats-Smith model attempts to represent small-scale heterogeneity of the porous medium.

Unfortunately, there is no simple method to measure f and α independently; rather, a "best fit" of displacement parameters f , Pe and α is determined by parameter estimation techniques applied to effluent composition data.

A comprehensive discussion of the precision of Coats-Smith parameter measurements, parameter sensitivity, and dependency of the parameters on flow velocity is given by Orr and Taber (1984). The remainder of this thesis is an attempt to relate observations of pore structure to the values of f , Pe and α .

Mixing in Rocks

Mixing during displacements in a reservoir core must be strongly influenced by the structure of the pore network. The structure of the pore network, in turn, is determined by the composition and distribution of constituent rock components. Development of pore system structure in a rock, then, is ultimately controlled by a combination of depositional and diagenetic processes which occur over geologic time (see Chapter 4).

Features of reservoir pore structure which influence mixing occur in a wide range of sizes; at the interwell scale facies changes, fractures and less common features such as cavernous porosity affect displacement performance. On the

microscopic level, mixing is affected by local heterogeneities of pore structure. In the discussion that follows, petrophysical factors which affect mixing at the pore level are examined. Though large-scale reservoir features are not considered here, this study represents a first step toward relating flow behavior to reservoir petrology.

In traditional petrophysical analysis of pore systems, properties such as porosity, permeability, pore size and shape, coordination number (the number of pores connected to a reference pore) and aspect ratio (the ratio of pore body size to pore throat size) are considered. While it is clear that each of these properties exerts some influence on flow phenomena, individually, none of them seems likely to control mixing behavior. For instance, it is easy to envision two rocks which have approximately equivalent values of porosity and permeability but exhibit totally different mixing behavior. Pore size alone also seems unlikely to strongly influence mixing. Consider two geometrically similar pore systems differing only in average pore size. It is likely that miscible displacements in these systems would produce similar effluent composition profiles as long as the flow velocity was low enough to allow diffusion to equalize concentrations within typical pores (Orr and Taber, 1984). Pore shape and pore wall roughness must play some role in fluid mixing, but if pores, on average, are small enough, or flow is slow enough, that

diffusion can equalize concentrations within them, it is not clear that convoluted, polyhedral pores would produce results very different from those of smooth, spherical pores.

Aspect ratio and pore coordination number have been shown to strongly affect fluid distribution when capillary forces are important (Wardlaw, 1980, Chatzis et al., 1982), but it is not clear how they influence mixing in single-phase miscible displacements.

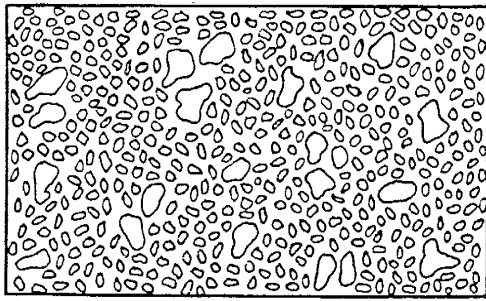
Carman (1939) reasoned that for a porous rock, the average flowpath is 45° to the direction of displacement. Flowpath tortuosity has an influence on transition zone development during a displacement (Orr and Taber, 1984). It is hypothesized, then, that a relation exists between the dispersion coefficient (a reflection of the size of the transition zone) and the mean flowpath orientation, as determined by vector analysis of pore structure in thin section. An inherent assumption here is that a mean flowpath normal to the direction of displacement would produce a higher dispersion coefficient than one resulting from a mean flowpath parallel to the longest axis of the core.

One property which clearly does influence mixing is the pore size distribution. Spence and Watkins (1980) found that displacements in samples with wide pore size distributions resulted in flowing fractions of less than one. It is useful here to reconsider the definition of

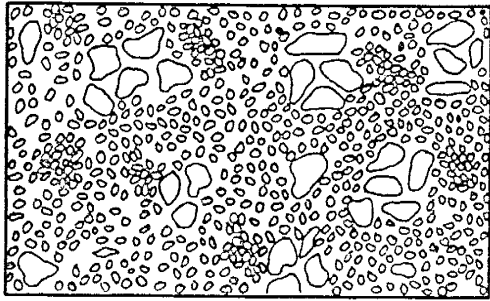
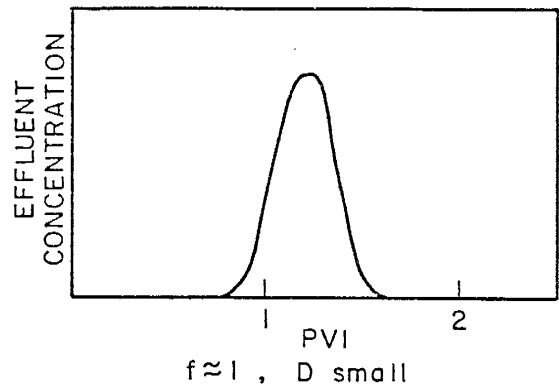
flowing fraction in order to better understand the significance of the pore size distribution.

Flowing fraction (f) is defined by Coats and Smith (1964) to be the fraction of total pore volume in a porous medium which is occupied by mobile fluid. This idealization implies that some of the pore volume contains immobile fluid, but this is not necessarily the case. Spence and Watkins (1980) argued that fluid need not be strictly stagnant to be included in the nonflowing fraction. Instead, it need only flow significantly more slowly than fluid in other portions of the pore space. The distinction to be made here is that fluids which comprise the "main flowing stream" in a displacement are considered to be the fluids which move at relatively high velocities through large, well-connected pores and fractures. "Dead-end pore volume" (Coats and Smith, 1964) is actually restricted pore volume in which fluids move slower due to smaller pore size, greater flowpath tortuosity, and constrictions or obstructions between pores.

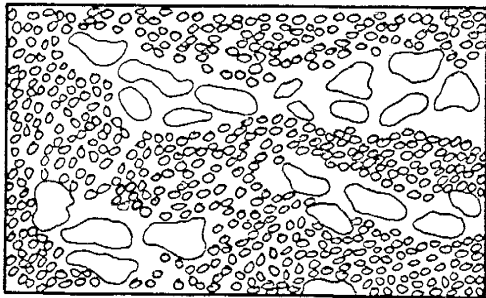
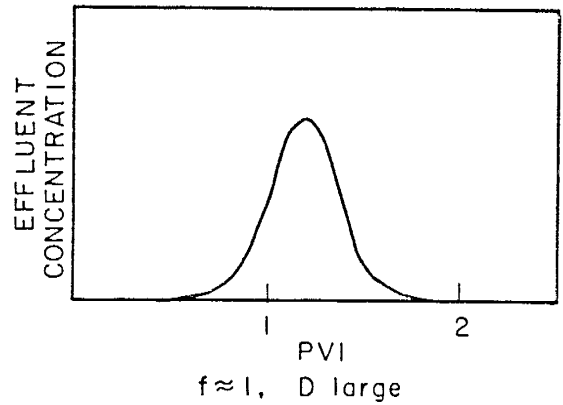
It follows, then, that a flowing fraction of less than one may indicate the existence of preferential flowpaths in the rock. If true, then a wide distribution of pore sizes may be associated, at least loosely, with preferential flow channels. It seems likely, however, that a wide pore size distribution does not guarantee a flowing fraction of less than one. Figure 2.2 shows four idealized pore systems with the same pore size distribution but very different flow



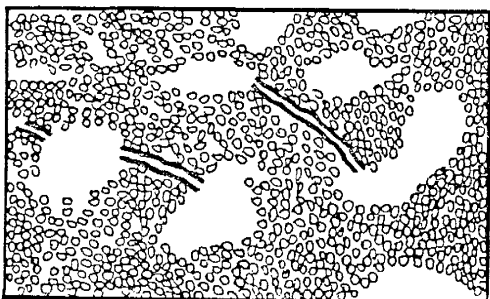
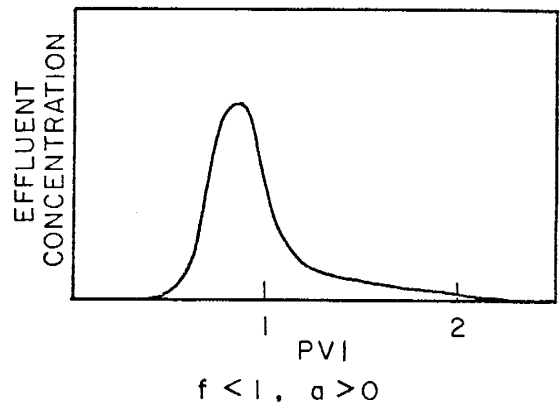
a. RANDOM DISTRIBUTION OF
LARGE AND SMALL PORES



b. RANDOM DISTRIBUTION OF
CLUSTERS OF LARGE AND
SMALL PORES



c. NONRANDOM DISTRIBUTION
OF CLUSTERS OF LARGE
AND SMALL PORES



d. FRACTURES AND VUGS

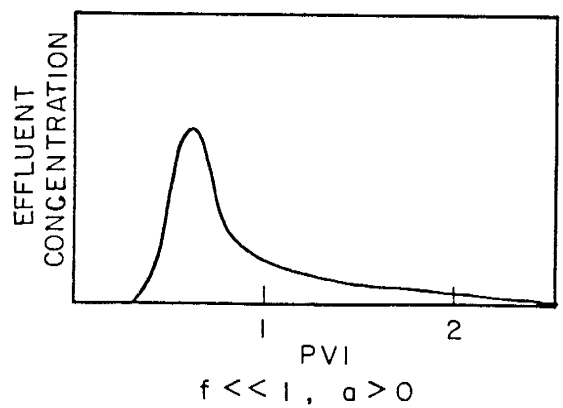


Fig. 2.2 Idealized Pore Systems

behavior. In Figure 2.2a, the large and small pores are randomly distributed. Flow in such a system would be characterized by a flowing fraction of one and a dispersion coefficient greater than that of a system of totally homogenous pores, but still relatively low. Figure 2.2b shows pores with the same size distribution, but a varied spacial distribution. The large and small pores are arranged in clusters, and the clusters themselves are randomly distributed so that no preferential flow paths exist for samples which are large compared to the scale of the clusters. Such a pore system would also have a flowing fraction of one, since local variations in flow would average out over a large-enough flow distance. The dispersion coefficient would be larger here compared to the previous case, a reflection of greater mixing due to the local flow variations.

In Figure 2.2c, another pore system containing clusters of large and small pores is shown. In this case, the distribution of clusters is not random. Preferential flow paths exist, and slower-moving fluids in smaller, restricted pores exchange by diffusion into these paths. Results of a displacement performed in this pore system can be characterized by a flowing fraction of less than one, dispersion in the main flowing stream, and mass transfer between restricted and flowing streams. The fourth idealization (Fig. 2.2d) represents a variation of the preceding pore system. The pore structure contains

fractures, vugs, and matrix micropores. Again, this system leads to very early breakthrough of the displacing fluid and therefore a value of f which is much less than one. This configuration most closely approximates the pore structure envisioned in the Coats-Smith model.

These idealized pore systems suggest that a wide pore size distribution alone is not sufficient to produce low flowing fractions. The pore space must also be connected in ways which result in preferential flow paths on the scale of the displacement.

CHAPTER 3

SAMPLE EXAMINATION METHODS

This chapter presents the methods of core examination and data collection employed in this study. Seven core samples were examined: three sandstones of various ages from Ohio, Wyoming and West Virginia, and four San Andres Formation (Permian) dolomites from New Mexico and West Texas. All of the samples were studied in hand sample, thin section, and by X-ray diffraction. Insoluble residue analysis was performed on the four carbonates; selected samples were examined on the SEM. A number of techniques were employed to study pore structure and are described below.

Whole Core Analysis

Core samples were examined with a hand lens to determine presence of sedimentary structures, stylolites, and the general character of the rock. Porosity and permeability-to-air were reported by Orr and Taber (1984).

Thin Section Preparation

At least three thin sections of each sample were examined under the petrographic microscope. Limited availability of certain samples required such a minimum; additional thin sections were cut from larger samples. One

thin section of each sample was cut normal to the assumed bedding plane to establish the presence or absence of sedimentary structures and vertical changes in grain-size distribution. The other two thin sections were cut parallel to the axis of the core used in the displacement experiment. Displacement cores were horizontal plugs taken from standard, vertical borehole cores. One of these sections was impregnated with colored epoxy to accentuate pore structure under the microscope.

Thin Section Petrography

Thin section microscopy provided information on types of constituent grains, cement and matrix, including mineralogy, size, shape, habit (crystals) and packing structure. The diagnostic stain Alizarin Red-S was used to identify calcite in the samples. Three-hundred-point counts were done on the slides; the results are tabulated in Appendix A.

Data which characterize pore system structure were obtained from photomicrographs of the samples and from direct observation under the microscope. Pore size distributions were determined by a previously undescribed method of point counting, herein named the "Union Jack" method. Using a very fine lead, a series of lines were drawn across the face of a thin section, resulting in a pattern resembling that of the British flag (Figure 3.1), hence the name. During a traverse of these lines under the

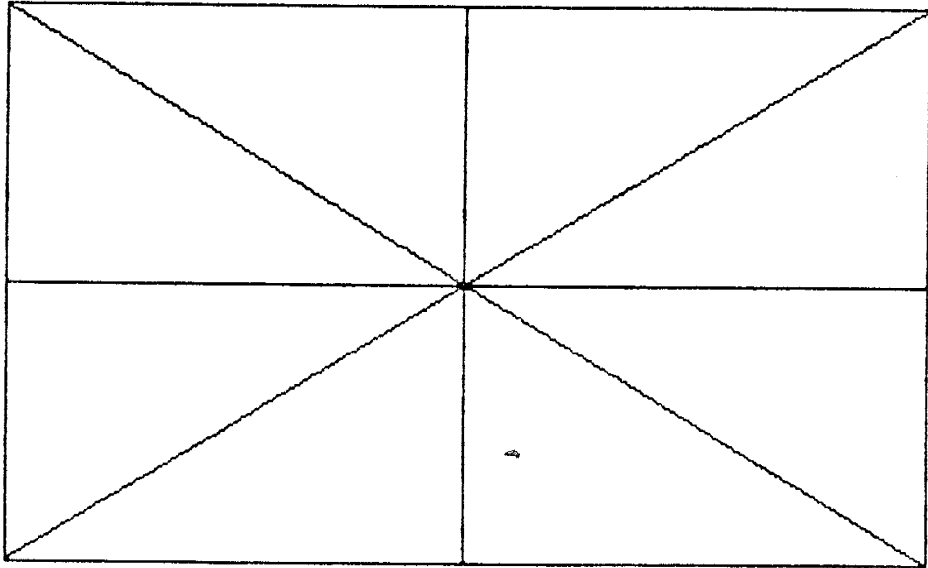


Fig. 3.1 "Union Jack" Configuration

microscope, between three-hundred and five-hundred pores were measured and categorized by size. This method offers no distinct advantages over other point-counting methods; it was adopted for convenience in lieu of an automated microscope stage.

Pore size was defined to be the diameter of the smallest circumscribing circle which can be drawn around a pore. This definition was adopted for simplicity in view of the number of measurements required per thin section. This method of pore measurement exaggerates the diameter and volume of the pore somewhat, because it is based on the longest dimension of the pore. Measurement of pore sizes in thin section partly compensates for this exaggeration because a random slice through a rock shows only a few pores which have been cut through their longest dimension. Further limitations lie in the failure to account for convoluted pore geometries, the attempt to describe 3-dimensional pore structure with essentially 2-dimensional thin sections, and in the subjectivity of the observer in determining the bounds of each pore measured. Every effort was made to measure pore sizes of each of the samples in a consistent manner.

Pore size distribution histograms were constructed by plotting the percent of total porosity contained in pores of a given size against that pore size. The histograms were constructed using the same scale of pore size for ease in comparison of results between samples. In the case of

dolomite sample M1, an additional, larger-scale histogram was necessary due to the very wide distribution of pore sizes in that sample.

Scanning Electron Microscopy (SEM) and Energy-Dispersive X-Ray Analysis (EDX)

The SEM was used to characterize the nature of pore-throat structure and identify pore-lining clay minerals. The EDX was employed to identify mineralogies of unknown grains and crystals. Tiny (~1.0 cm) chips of sample were glued onto disc-shaped steel mounts with epoxy. The samples were coated with silver to enhance electrical conductivity and then run on the SEM at 20.0 kV over a variety of magnifications. Due to operational problems with the SEM, only half of the samples studied were examined with this analytical tool.

X-Ray Diffraction of Clay Minerals

Identification of clay minerals in the samples was accomplished by use of X-ray diffraction. Clays occur in all of the studied sandstones but in none of the carbonates. A detailed treatment of the X-ray diffraction techniques employed is found in Grim (1968). X-ray diffraction data are found in Appendix A.

Flowpath Vector Analysis

Some measure of the tortuosity of a pore network may be determined by examining the average flowpath orientation within the system. Mean flowpath orientation might be related to dispersion coefficient, as discussed in Chapter 2.

The procedure for determining mean flowpath vectors is identical for both sandstones and carbonates. Two 8" x 10" photomicrographs of each sample were oriented with respect to the direction of displacement (0°). Each sample was photographed at a constant magnification to permit comparison of results. After placing a photo on a table, a brad was dropped onto the print to randomly determine which pore was to be examined. When the brad landed on a pore, the path from the reference pore center to the center of a connected, nearest-neighbor pore was described by means of a series of vectors measured relative to the direction of displacement. In cases where more than one pore was connected to a reference pore, pores which connected toward the displacement direction were measured (Fig. 3.2).

Fifty flowpath orientations were recorded from each photograph, giving a total of one-hundred flowpath orientations per rock sample. Mean flowpath orientations ($\bar{\theta}$) and vector strengths (\bar{r}_f) are tabulated in Table 5.3.

One limitation of this method is that 2-dimensional pore representations were used to infer 3-dimensional pore structure in the rock samples. This probably causes a significant amount of measurement error.

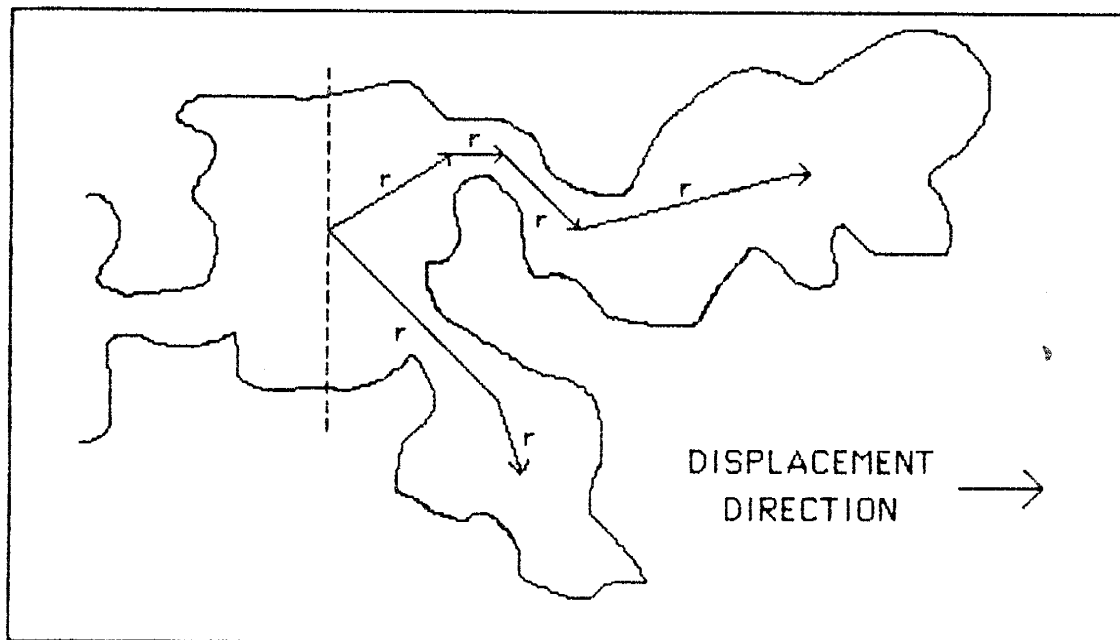


Fig. 3.2 Flowpath Vector Analysis Method

Spatial Distribution of Pores

Photomicrographs described in the preceding discussion of vector analysis were re-examined in an effort to determine if spatial pore distributions, that is, the manner in which pores of a given size are connected to similarly- or variably-sized pores, show trends which are useful in the interpretation of miscible displacement results.

The procedure involves random selection of a reference pore in the same manner as was done for the vector measurements. A semicircle with diameter (base) equal to three times the mean pore size of the sample was drawn on the photo (Fig. 3.3). Table 3.1 contains the mean pore sizes of the samples used in the construction of the semicircles. Three times the mean pore size was chosen as the diameter of the semicircle with the hope that a representative sample of proximal pores could be obtained. The center of the base of the semicircle was passed through the center of the reference pore; the base was drawn normal to the direction of displacement, and the arc was oriented in the displacement direction.

All pores within the semicircular area were counted and their diameters measured whether or not they appeared to be directly connected to the reference pore. A mean size of these neighboring pores was then determined. The above procedure was repeated for fifteen randomly chosen reference pores measured from photos of each sample. Fifteen was

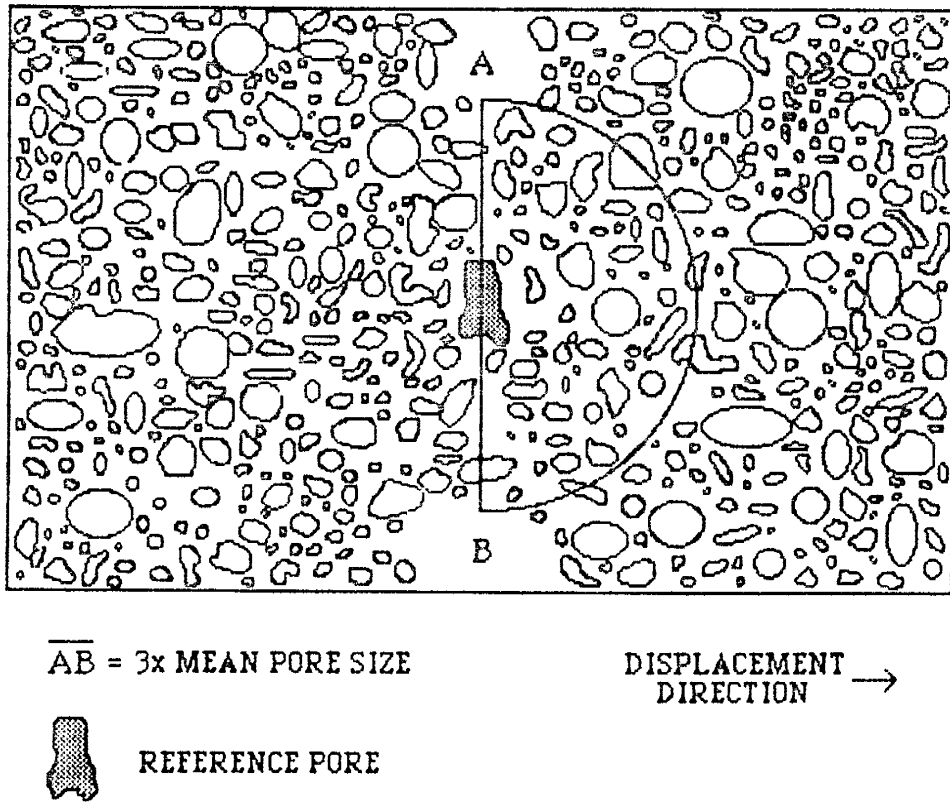


Fig. 3.3 Method of Determining the Spatial Distribution of Pores

TABLE 3.1 Mean Pore Sizes Used in Construction of Spatial Pore Distributions

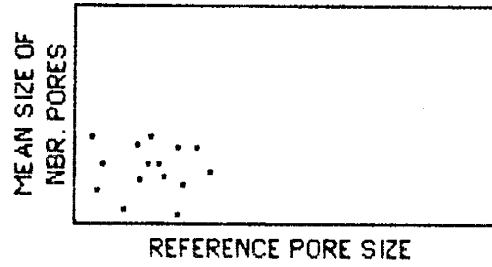
<u>Sample</u>	<u>Mean Pore Size (μ)</u>	<u>3x Mean Pore Size (μ)</u>
B1	169.44	508.32
F2	108.48	325.44
R1	259.80	779.40
WW2	343.23	1029.69
H1	471.91	1415.73
SAO	440.29	1320.87
M1	1131.58	3394.74

chosen as the number of reference pores to be examined because it seemed sufficiently large to adequately represent the pore structure of the the samples while not requiring excessive time for measurement. The reference pore sizes were then plotted against the mean size of neighboring pores. The results are presented in Chapter 4. If such distributions are random (Fig. 3.4a), where pores of any size are proximal to pores of many other sizes, than the existence of preferential flowpaths in the core is unlikely, since preferential flow is assumed to occur primarily in large, well-connected pores, though some small pores may participate also. If a trend exists in which small pores are connected primarily to small pores and large pores to other large pores (Fig 3.4b), preferential flow is a likely possibility.

Single-Phase Displacements

Single-phase displacements reported by Orr and Taber (1984) were performed at a nominal 10 ft/day rate in three sandstone and four carbonate cores. Miscible fluids of matched density and viscosity were used to minimize the effects of variable fluid properties on the development of the transition zones within the cores. A detailed treatment of the experimental procedure is given in Orr and Taber (1984). Briefly summarized, a core of known pore volume is initially saturated with a fluid. Injection of a slug of displacing fluid is achieved using a Teflon sample loop of

a. RANDOM DISTRIBUTION OF PORE CONNECTIONS



b. CONNECTIONS BETWEEN LIKE-SIZED PORES

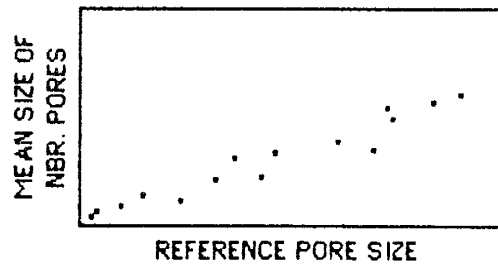


Fig. 3.4 Typical Spatial Pore Distributions

known volume. The displacing fluid differs from the displaced fluid by the addition of a tracer, typically sucrose. The effluent fluid mixture passes through an on-line refractive index detector which produces a linear response to sucrose concentration. The concentration of one fluid with respect to the second fluid can be determined for any point in time during the displacement. Data is plotted as concentration vs. pore volumes injected; a typical curve would be similar to that shown in Figure 2.1. Since the pump (flow) rate is held constant during the experiment, the "pore volumes injected" axis is equivalent to a "time" axis. Results of these displacements are tabulated in Table 5.1.

CHAPTER 4

PETROLOGIC ELEMENTS RELATED TO POROSITY AND PERMEABILITY DEVELOPMENT

The structure of pore systems in reservoir rocks is related to the composition and structure of the rocks themselves. Pore network development is controlled by a complex interaction of physical and chemical processes which operate over geologic time. This chapter discusses the development of porosity types which occur in the sandstones and carbonates studied.

Geologists loosely group reservoir porosity into two types. Primary porosity refers to voids which are present at the time of sediment deposition. Secondary porosity indicates voids which exist as the result of diagenetic processes, such as fracturing and dissolution.

Pore Development in the Sandstone Samples

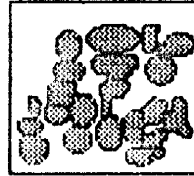
In sandstones, primary porosity occurs primarily as intergranular voids, but also as micropores between detrital clays, if they are present. The structure of intergranular pores is dependent on the shape, size, sorting and packing of the grains. Well-developed primary porosity (Fig. 4.1a), if not destroyed during diagenesis, is often associated with high permeability.

Diagenetic processes which reduce porosity and permeability include compaction, pressure solution and

a. POINT CONTACTS



b. LINE CONTACTS



c. CONCAVO-CONVEX CONTACTS



Fig. 4.1 Grain Contacts in Sandstones

cementation. Figure 4.1b is a schematic sketch of the combined effects of compaction and pressure solution on intergranular porosity. Regular intergranular pore texture, characterized by point contacts between grains, alters to a texture with line and concavo-convex contacts, and lower porosity and permeability.

Other diagenetic processes serve to enhance porosity. These include dissolution of grains and cements, chemical alteration of grains (i.e. feldspar altered to clay minerals), and fracturing. Dissolution of detrital grains, authigenic cements and replacement minerals (Figs. 4.2a-c) is common and individual sandstones often contain a combination of dissolution-pore types (Pittman, 1979).

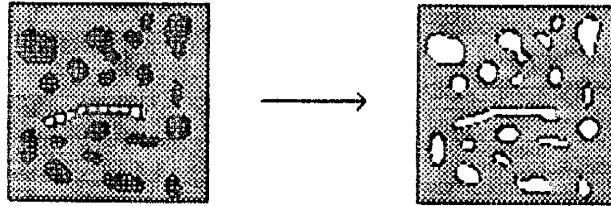
Micropores occur in sandstones among clay mineral interstices or at pore-throat constrictions. Authigenic clays may precipitate directly from pore fluids or as a result of chemical destruction of in situ feldspar grains.

Fracturing (diagenetic or artificially induced) provides additional permeable flow paths. In rocks with well-developed primary porosity and permeability, the effect of fractures on flow is small compared to rocks with lower initial permeability (Fig. 4.2d).

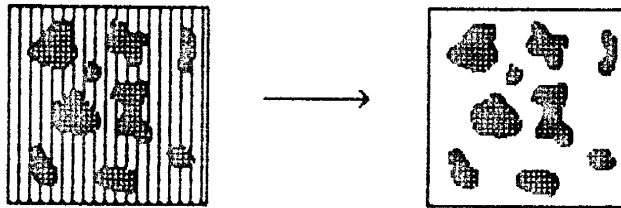
Petrology and Pore Structure of the Sandstone Cores

The Berea sandstone (sample B1, Figure 4.3) is a very-well-sorted sublitharenite of Mississippian age. The mean grain size lies on the boundary between medium and fine

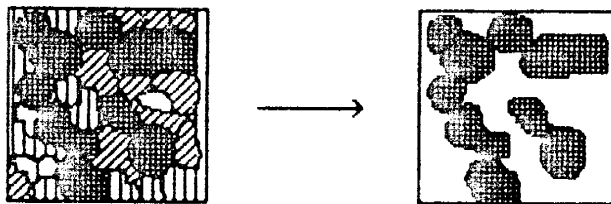
a. DISSOLUTION OF SEDIMENTARY MATERIAL



b. DISSOLUTION OF AUTHIGENIC CEMENT



c. DISSOLUTION OF AUTHIGENIC REPLACEMENT



d. FRACTURING

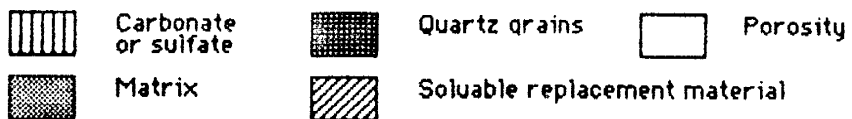
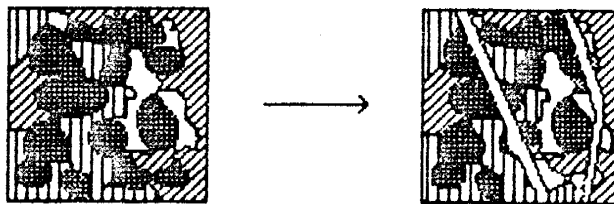


Fig. 4.2 Secondary Porosity in Sandstones

(after Schmidt and McDonald, 1979)



Fig. 4.3 Photomicrograph of Bl
Pores are colored blue.
Magnification: 25x

sand; the grains are subangular to subround and are primarily in point-to-point contact (Fig. 4.1a). Both primary intergranular and secondary dissolution pores are present. Incomplete precipitation of dolomite followed by its dissolution resulted in small patches of pore-filling dolomite cement distributed sparsely and randomly throughout the rock. Similarly, tiny crystals of pore-lining clay minerals (illite and kaolinite) are sparsely distributed in the sample.

The distribution of pore sizes for core B1 is shown in Figure 4.4. Pore sizes are distributed in a single, narrow mode, a function of the grain sorting and preservation of primary intergranular porosity. Angular pore geometries reflect the subround average grain shape. Pores less than 80 microns are mostly intergranular pore throats. Spatial distribution of pores appears to be random (Fig. 4.5), indicating that existence of preferential flow paths is unlikely.

The Frannie sand (sample F2, Figure 4.6) is a poorly-sorted subarkose with grain sizes which range from very fine (70%) to medium. As in the Berea, Frannie grains are subangular to subround, but they show signs of grain dissolution in line contacts (Fig. 4.1b) and enlarged pores. About 10% of the grains contain fractures which, in thin section, appear to be open.

Figure 4.7 shows the distribution of pore body sizes in the Frannie. The small grains and poor sorting are

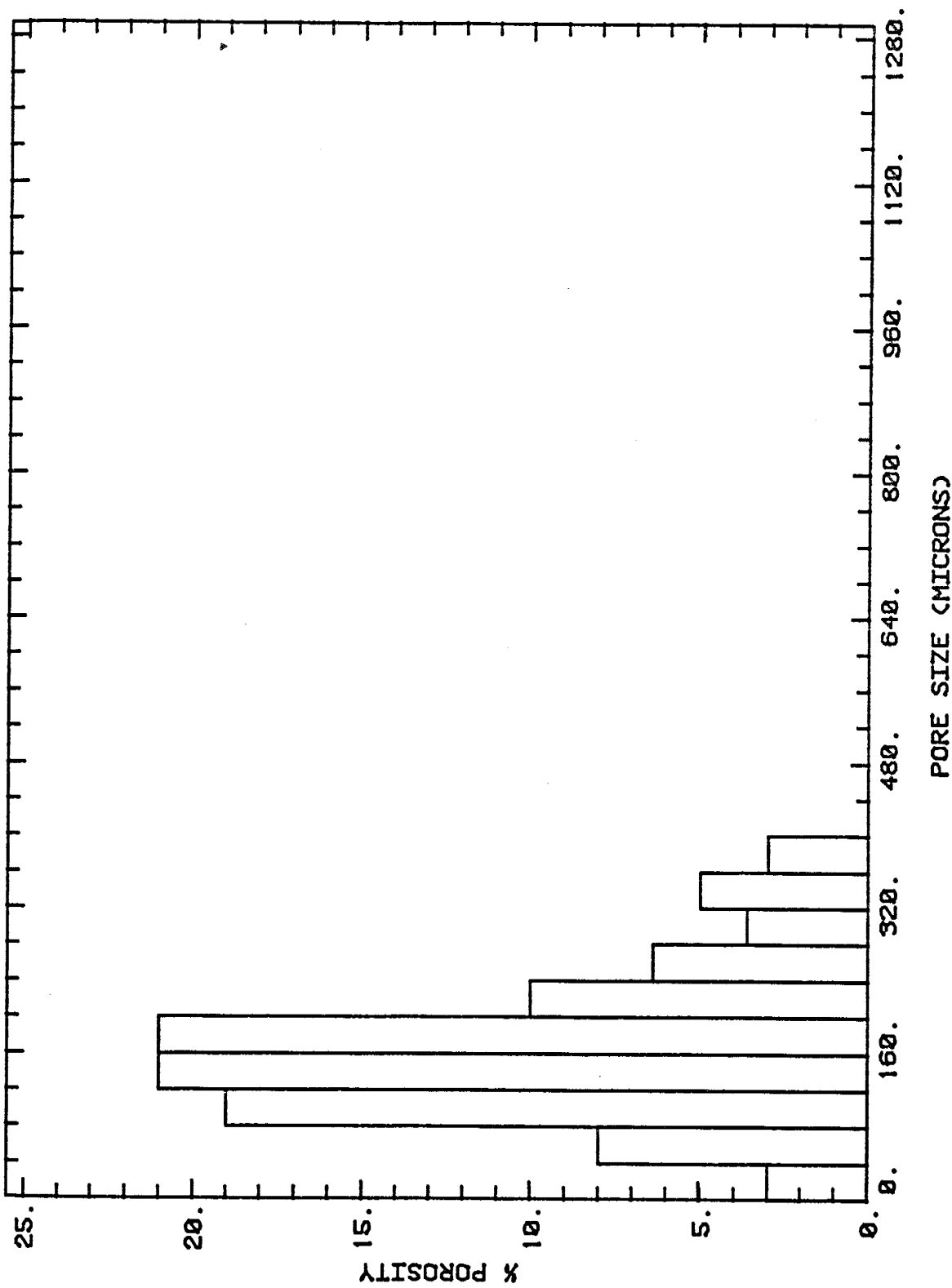


Fig. 4.4 Distribution of Pore Body Sizes for BI

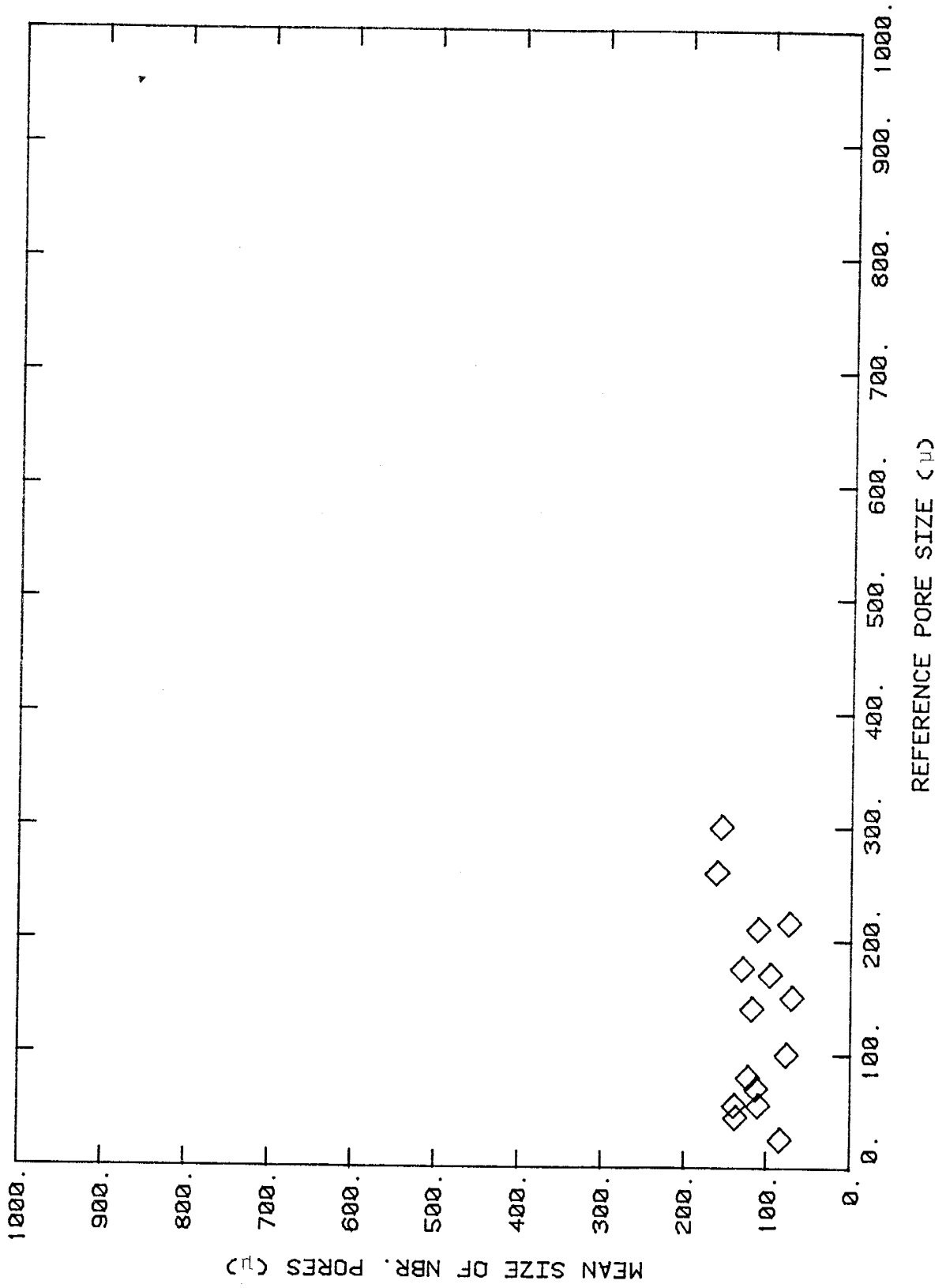


Fig. 4.5 Spatial Distribution of Pores in BI

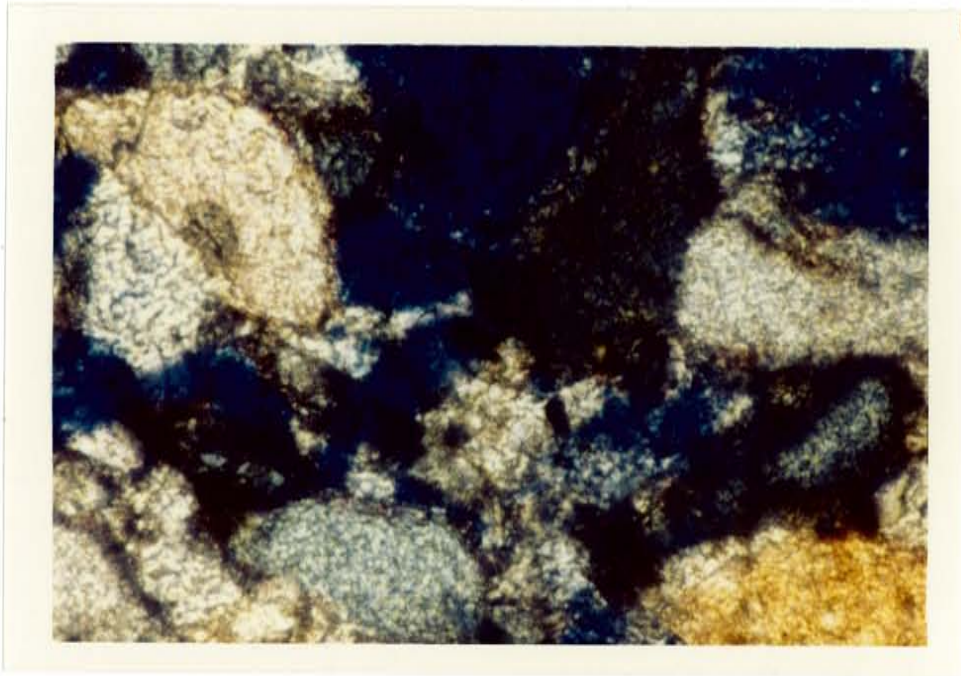


Fig. 4.6 Photomicrograph of F2
Pores are colored blue.
Magnification: 250x

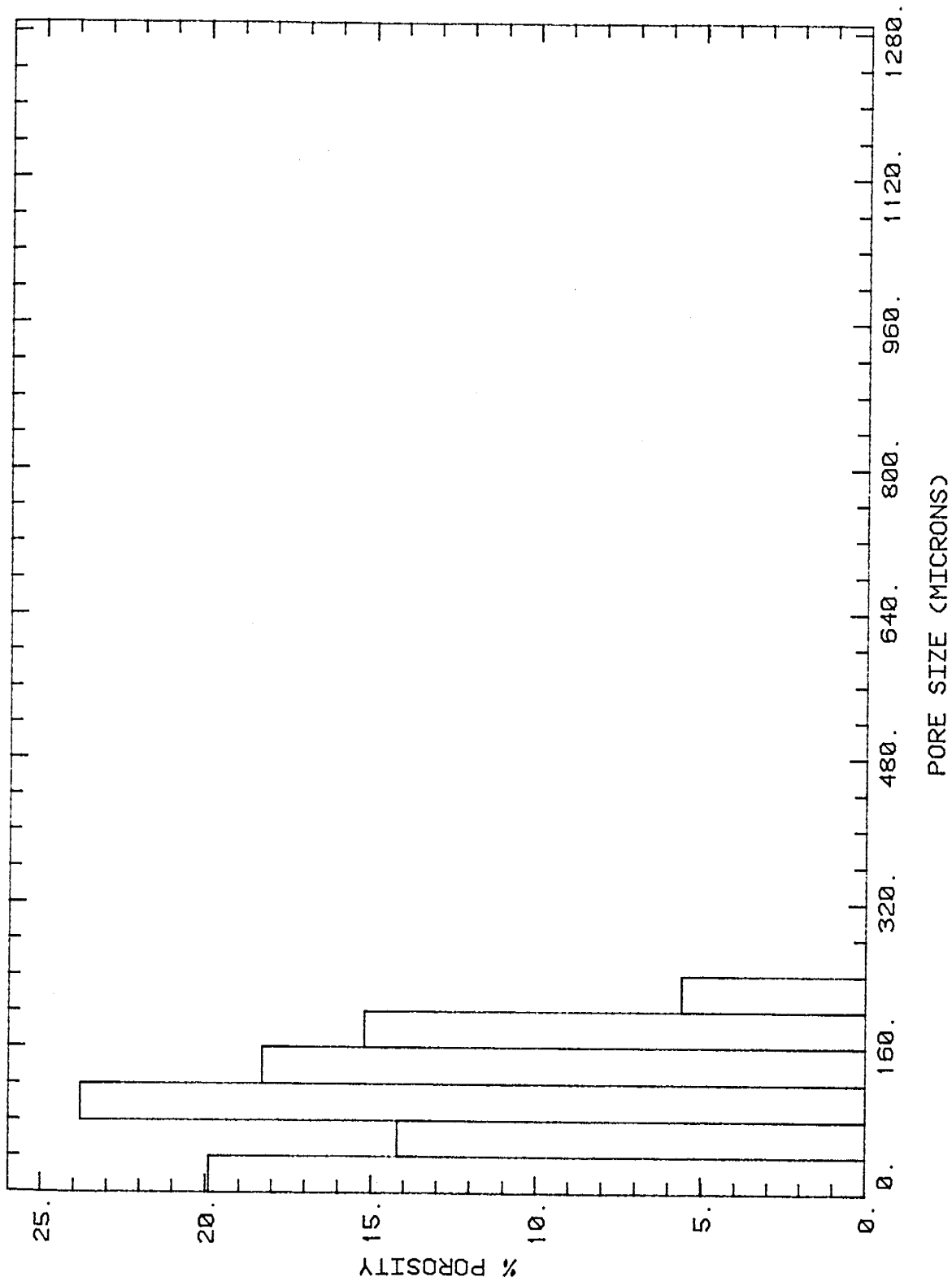


Fig. 4.7 Distribution of Pore Body Sizes for F2

reflected in the narrow distribution and small average pore size. Pore space is a combination of well-connected intergranular voids, secondary grain-dissolution pores and fractures. The spatial distribution of pores in F2 is shown in Figure 4.8. Like the data for B1, these data are random, which suggests that no preferential flow is likely.

In contrast to the Berea and Frannie samples, the Rock Creek sand (sample R1, Figure 4.9) contains a substantial amount of matrix in the form of micaceous laths (10%) and severely deformed feldspar (10%) embedded in masses of clay minerals (20%), specifically illite, vermiculite and kaolinite. The matrix is distributed as masses or "pods" around and between the angular, fine-sand quartz grains.

Development of pore structure in the Rock Creek sample is related to the dissolution and alteration of feldspar grains. Solution-enlarged cavities up to about 640 microns (Fig. 4.10) are distributed throughout the rock in a non-random fashion, a result of complete dissolution of some pre-existing grains and cements. The abundance of authigenic clays has given rise to abundant small voids and micropores.

The spatial distribution of pores in R1 is shown in Figure 4.11. The data are aligned in a weak linear trend; the coefficient of determination (r^2) is 0.72. Like-sized pores tend to be connected to each other, though sufficient scatter exists in the data to suggest that while preferential flowpaths may exist, they do not greatly influence displacement results.

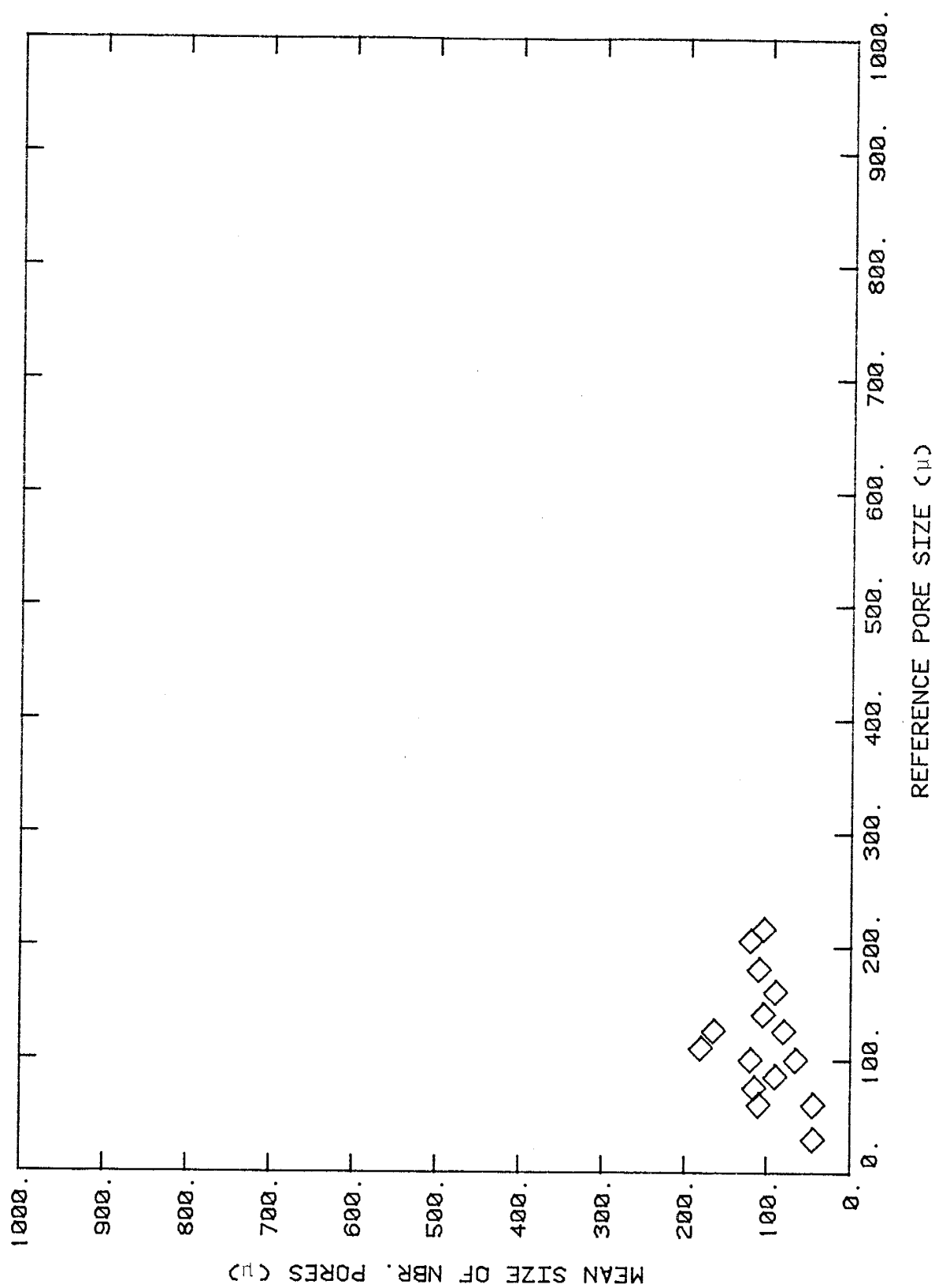


Fig. 4.8 Spatial Distribution of Pores in F2

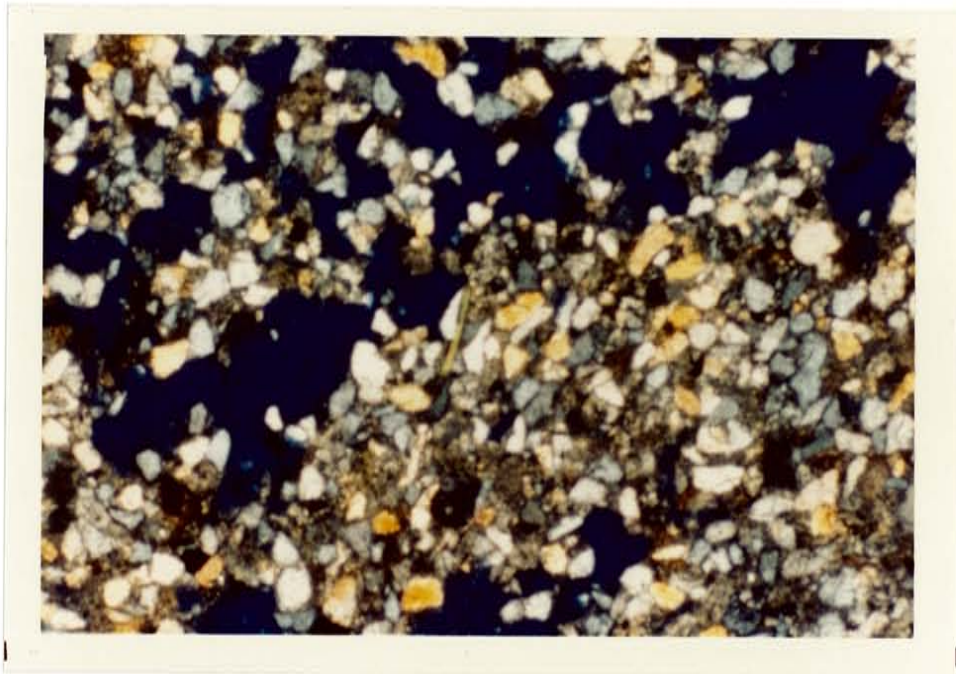


Fig. 4.9 Photomicrograph of R1
Pores are colored blue.
Magnification: 25x

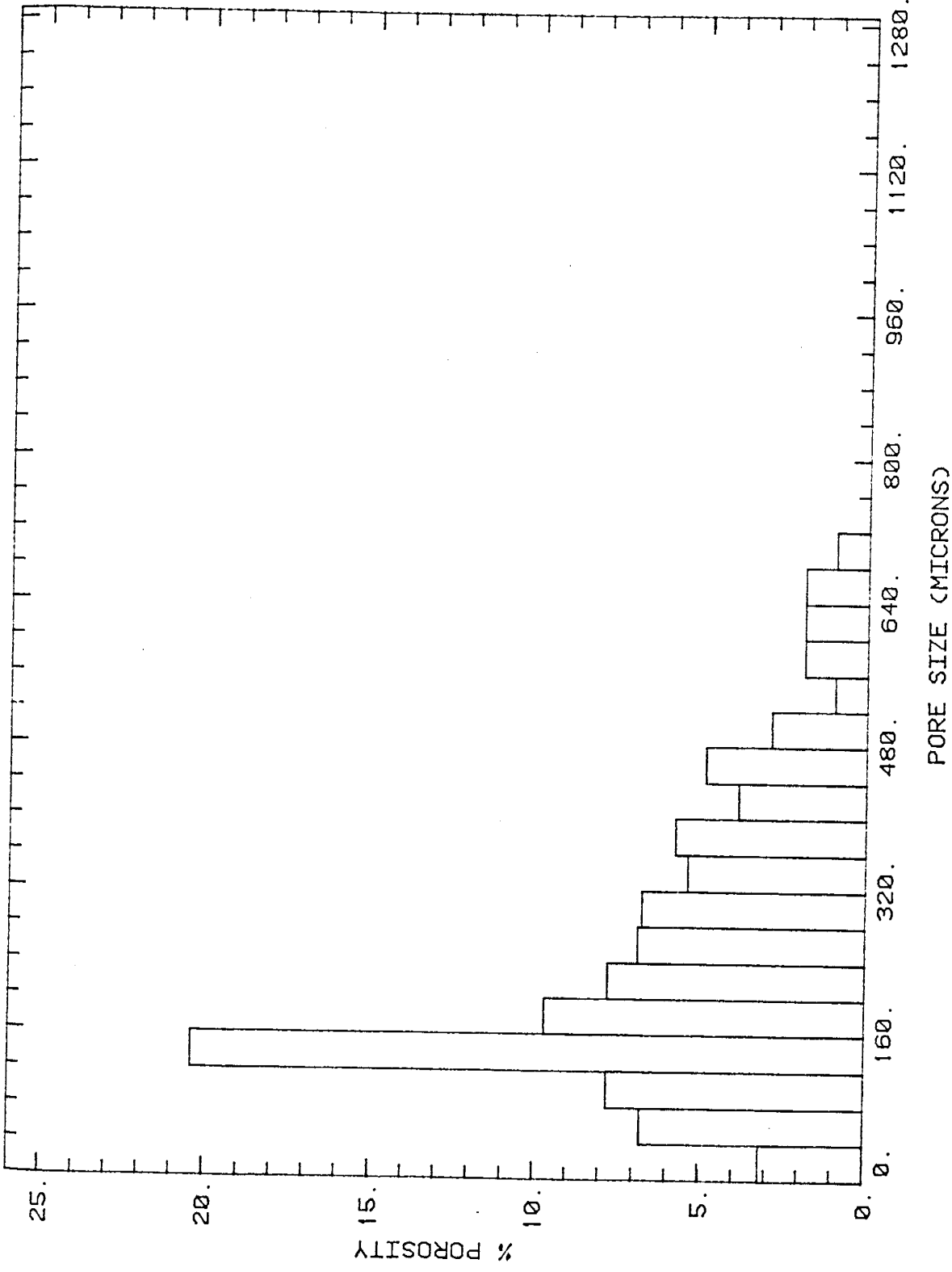


Fig. 4.10 Distribution of Pore Body Sizes for R1

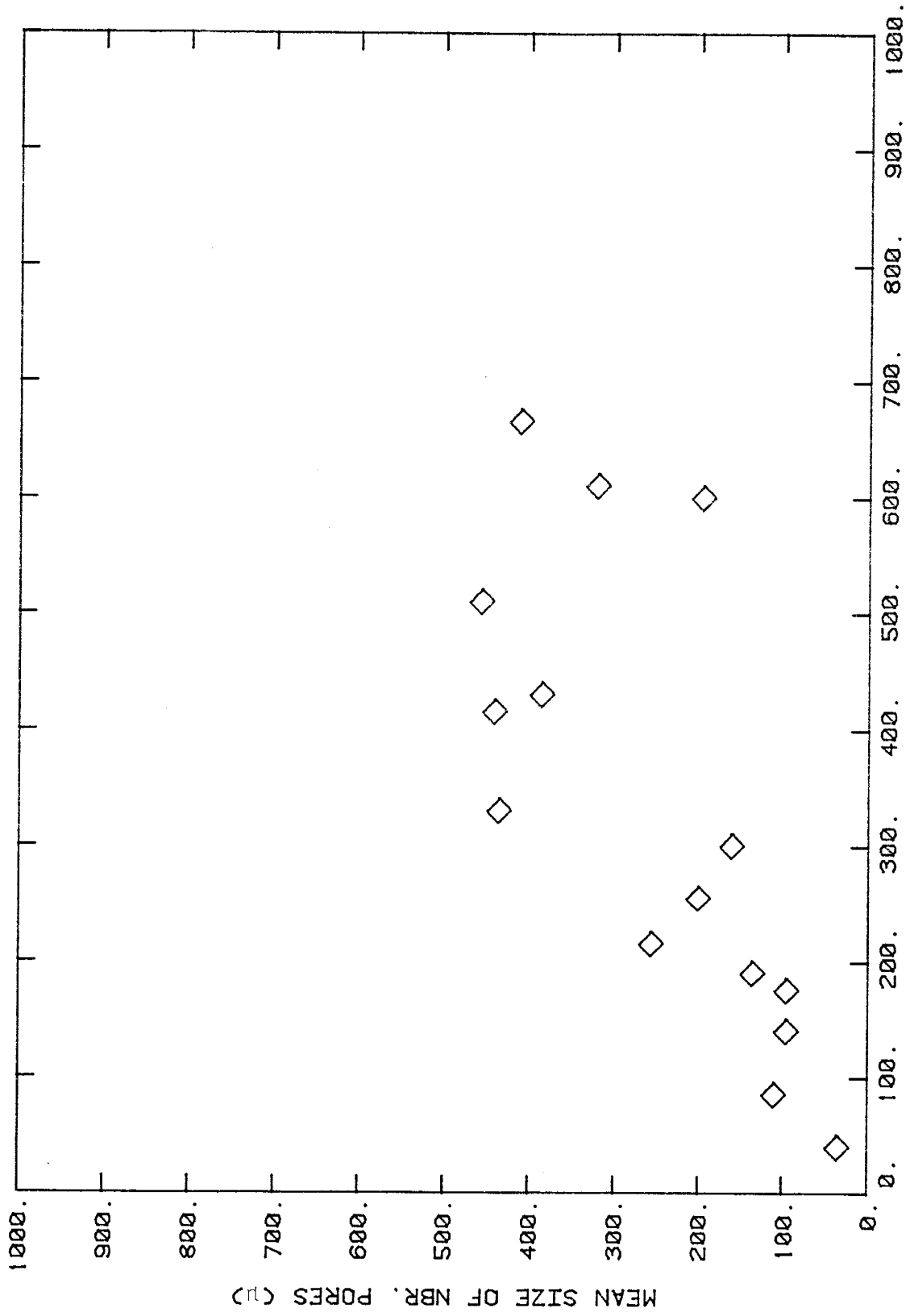


Fig. 4.11 Spatial Distribution of Pores in R1

Pore Development in the Carbonate Samples

Porosity and permeability development in the four San Andres Formation carbonates studied is due to a combination of depositional and diagenetic processes. In all four samples, the original sediment was probably composed of spherical ooid grains with primary intergranular porosity similar to that of an unconsolidated pack of spheres. Variable degrees of dolomitization and dissolution of pore-filling cements account for the differing pore structure among the samples.

Dolomitization of the San Andres was probably accomplished in two stages. Syngenetic dolomitization, similar to that described by Friedman and Sanders (1967), occurred under hypersaline conditions resulting from capillary concentration. Hypersalinity is indicated by the presence of anhydrite and anhydrite-crystal molds in the samples. Evaporitic sulfate precipitation increased the Mg/Ca ratio in the interstitial brines and thus induced dolomitization of the pre-existing calcium carbonate ooids, as described by Murray and Pray (1965). In addition to vugs formed from the leaching of anhydrite, the preservation of the original ooid fabric is evidence for syngenetic dolomitization having occurred.

All four samples in thin section show ooid fabrics preserved to some degree. Reservoir samples H1, WW2 and M1 have pervasive diagenetic dolomite which has all but

obliterated the primary fabric, leaving only ghost ooids visible in thin section. Outcrop sample SAO exhibits a well-preserved ooid fabric, and thus must not have experienced the effects of the second dolomitization stage.

The relationship between micropore geometry and growth of diagenetic dolomite has been discussed by Wardlaw (1976), who concluded that progressive changes in pore geometry occur as dolomite crystals grow, and that inhibition of crystal growth is of fundamental importance to the preservation of pore spaces in dolomites. His model of pore geometry development is that initial polyhedral pores are reduced to tetrahedral pores, which in turn may be eliminated to leave interboundary-sheet pores at the sites of compromise crystal boundaries. The occurrence of solid bitumen residues as intergrain sheets, and the relatively large volume occupied by interboundary-sheet pores in some dolomites, provides both direct and indirect evidence that these pores actually exist in the subsurface and are not the result of depressuring during core recovery (Wardlaw, 1976).

Petrology and Pore Structure of the Carbonate Cores

Pore structure in core WW2 (4.12) is more uniform than in any other carbonate sample, both in terms of size (Fig. 4.13) and spatial distribution (Fig. 4.14). As in the case of R1, no distinct trend can be determined in the spatial distribution data. These data appear to lie along a weak trend; the r^2 value for a linear fit is only 0.50.



Fig. 4.12 Photomicrograph of WW2

Matrix pores are colored black;
large vug is completely filled with
multicolored anhydrite.

Magnification: 25x

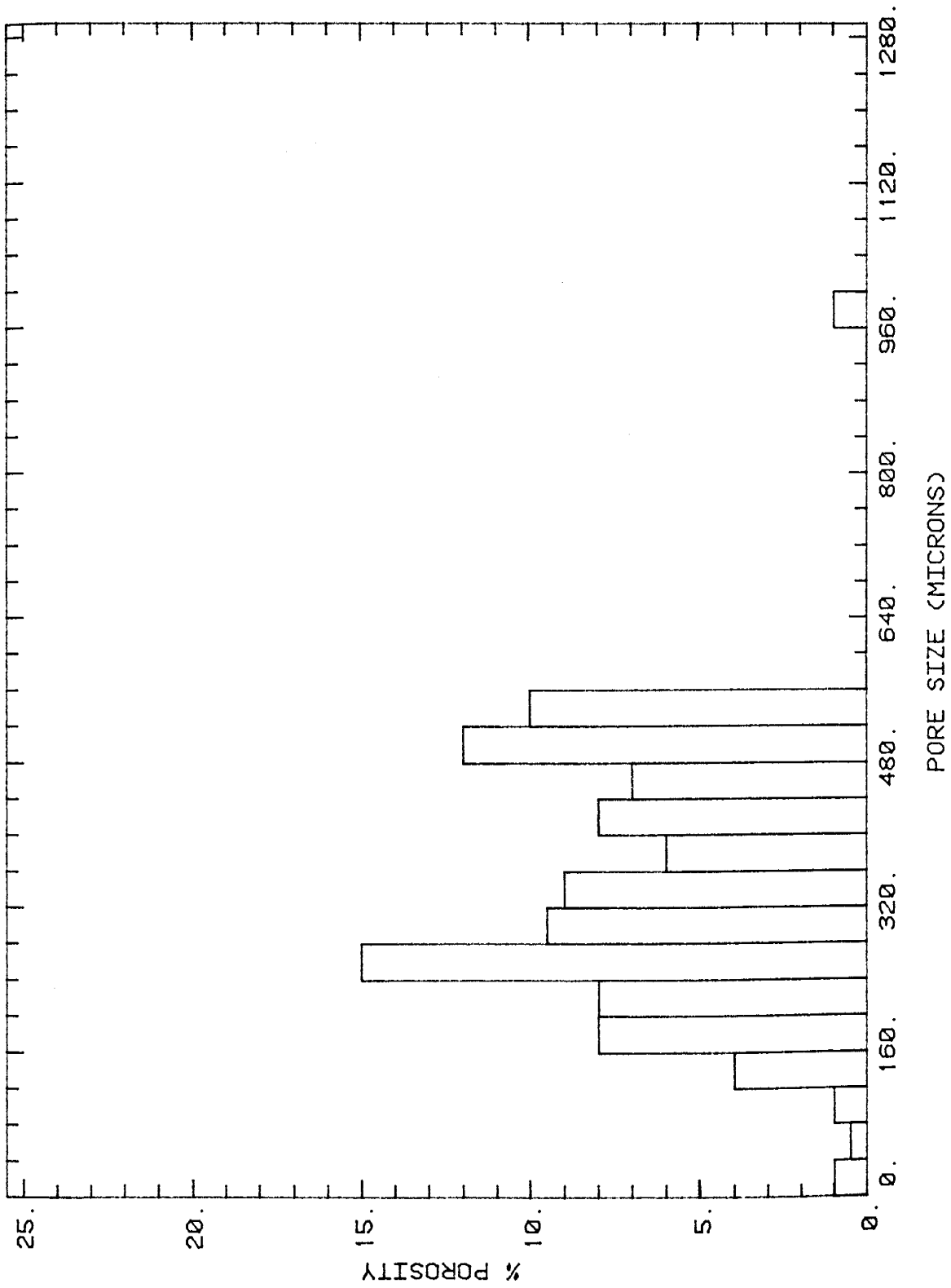


Fig. 4.13 Distribution of Pore Body Sizes for WW2

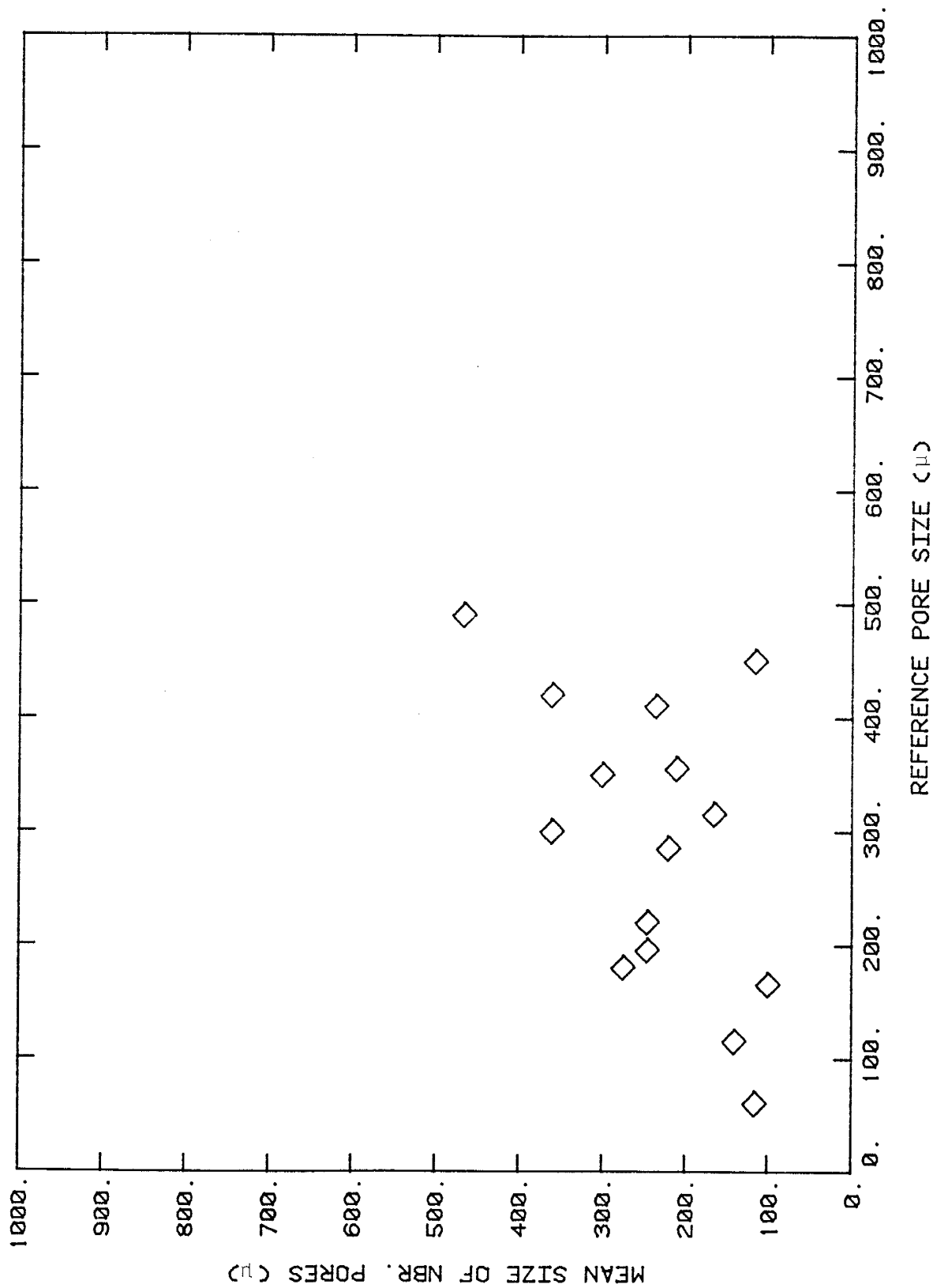


Fig. 4.14 Spatial Distribution of Pores in WW2

Dispersion of the data is sufficient to suggest that preferential flow through large pores does not occur in WW2. Pervasive diagenetic dolomite has nearly homogenized the matrix composition, and accordingly, the pore system structure. Some pore-filling anhydrite cement is randomly distributed through the rock, but it appears to have precipitated during a late diagenetic stage, since the dolomitization produced uniform, subhedral crystals throughout the rock.

Figure 4.15 shows the pore size distribution for Seminole core H1. The distribution is wider than the one characterizing WW2 (Fig. 4.13). This is due to the existence of medium and large vugs among the matrix micropores. Vugs are the result of replacement of aragonitic ooids by anhydrite during or preceding dolomitization, followed by dissolution of the replacement mineral. In the case of H1, not all of the anhydrite has been dissolved and removed. Figure 4.16 is a photomicrograph of H1 which shows two vugs. The one on the left is completely devoid of the precipitate, while the vug on the right is void except for the remnant anhydrite at the lower pore boundary. It is clear that this cement was in the process of removal since the crystal edges are degraded and irregular. Sulfate-dissolving brines which became saturated with sulfate lost their ability to dissolve anhydrite, resulting in selective vugular pore development, as shown in Figure 4.17. In this photo, the central vug is void, while adjacent vugs on each side remain anhydrite-

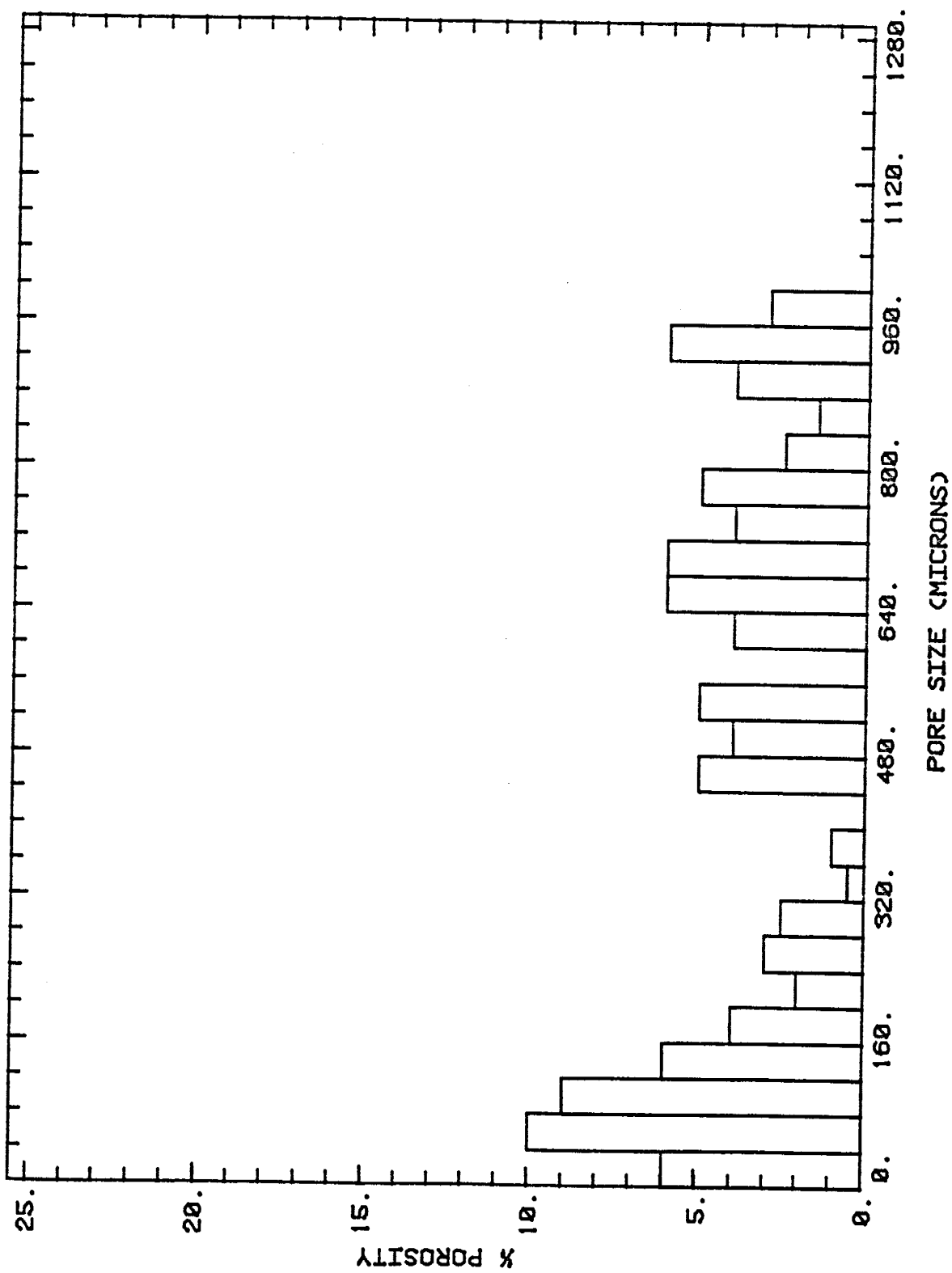


Fig. 4.15 Distribution of Pore Body Sizes for H1



Fig. 4.16 Photomicrograph of H1
Pores are colored black; remnant
anhydrite crystal sits on the lower
edge of the vug at the right.
Magnification: 25x

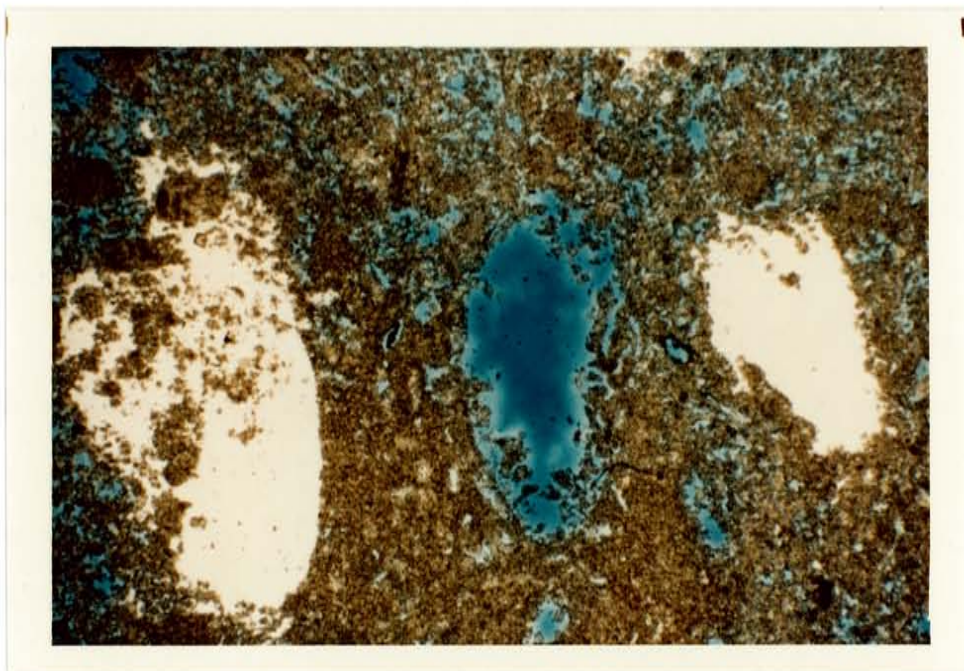


Fig. 4.17 Photomicrograph of H1
Pores are colored blue; white areas
are anhydrite plugs.
Magnification: 25x

filled. Anhydrite is also present in micropores adjacent to some vugs, reducing permeability locally.

Qualitative observations of permeability barriers and related preferential flow paths in H1 is supported by measurements of connectivity (Fig. 4.18). Smaller pores tend to be connected to like-sized pores, and that trend continues, if weakly, up through vugular pores.

Pore structure in core SAO (Figs. 4.19, 4.20) consists of solution-enlarged intergranular vugs, intragranular voids which occupy the centers of some ooids (Fig. 4.21), and a microporous fabric which pervades most of the dolomitized material. The solution cavities are the result of dissolution of grain boundaries along pre-existing primary flow paths combined with dissolution of ooid grains from the center outward. The dissolution of ooid centers ("oomoldic porosity") resulted from selective decay and removal of unstable nuclei (organic matter, for example). Syngenetic dolomitization created the intercrystalline micropore network.

Each genetic pore type is of a different size class. Intergranular channels are, on average, an order of magnitude greater in size than oomoldic pores which are at least an order of magnitude larger than the intercrystalline micropores; hence, the wide pore size distribution.

The spatial distribution of pores (Fig. 4.22) reflects the presence of oomoldic porosity. Voids in ooid centers are isolated from large intergranular pores by a sphere of

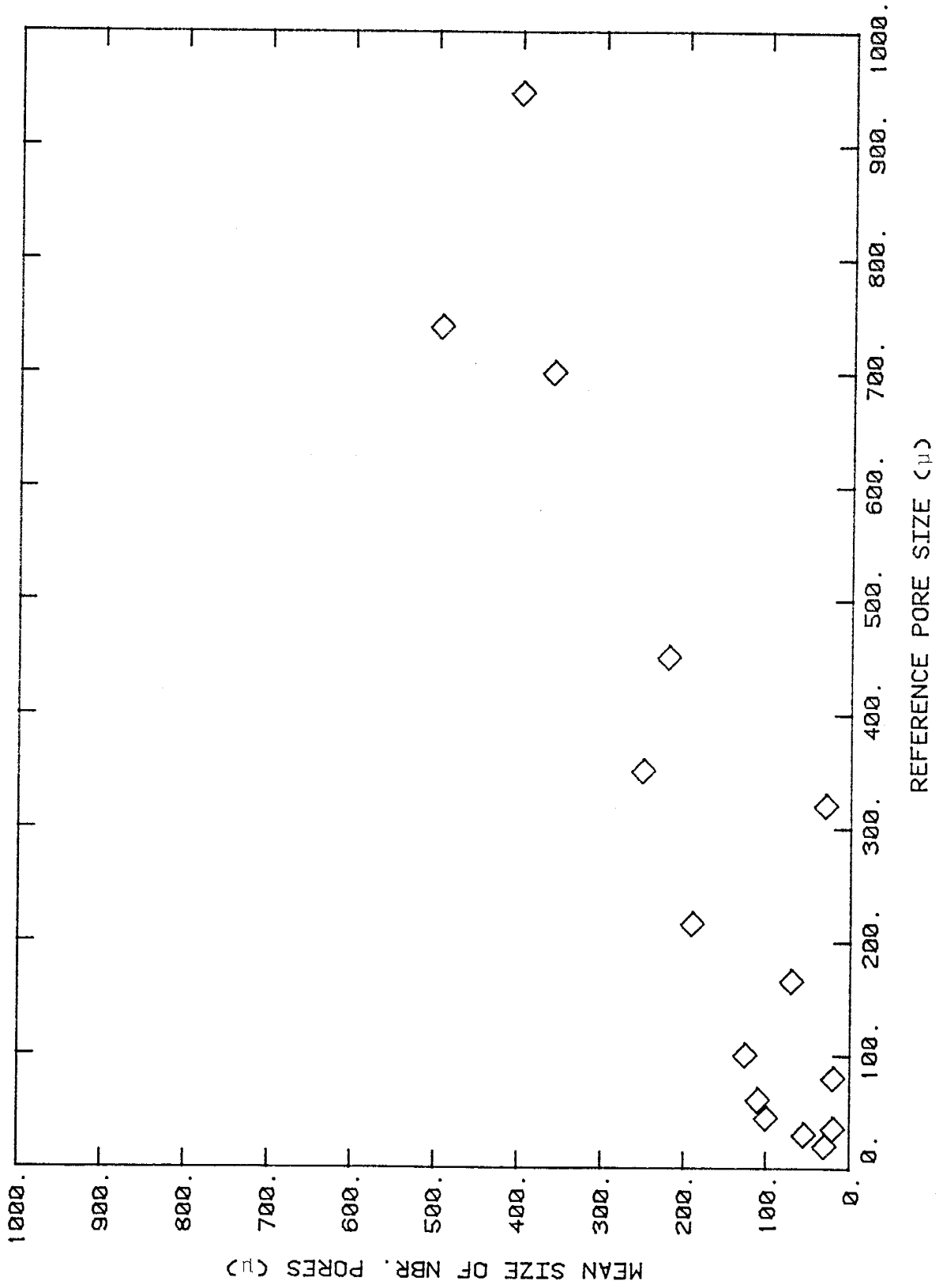


Fig. 4.18 Spatial Distribution of Pores in HI

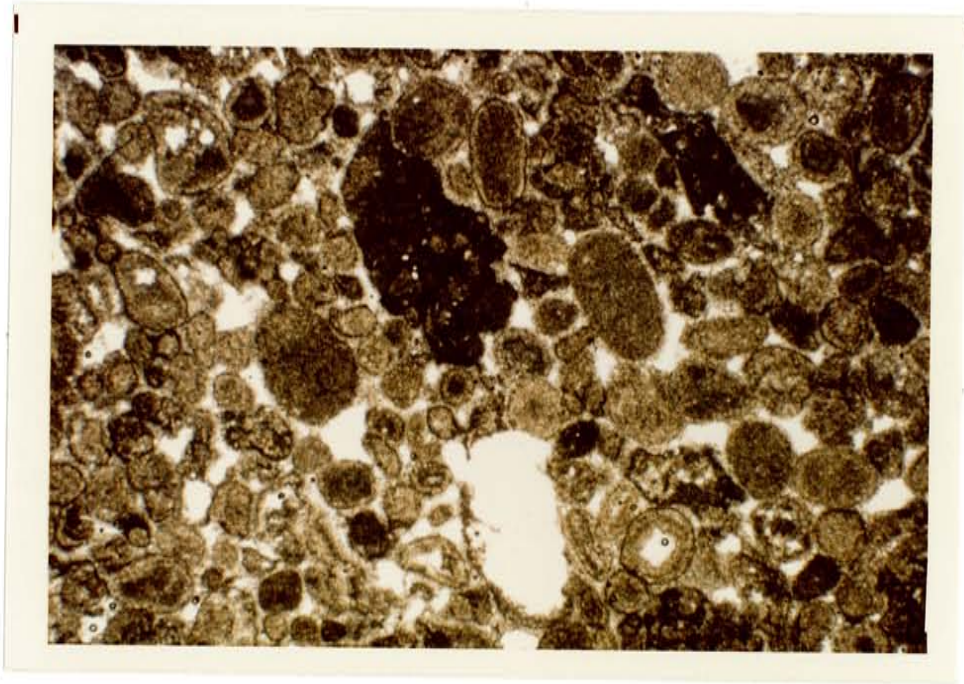


Fig. 4.19 Photomicrograph of SAO

Pores are colored white.

Magnification: 10x

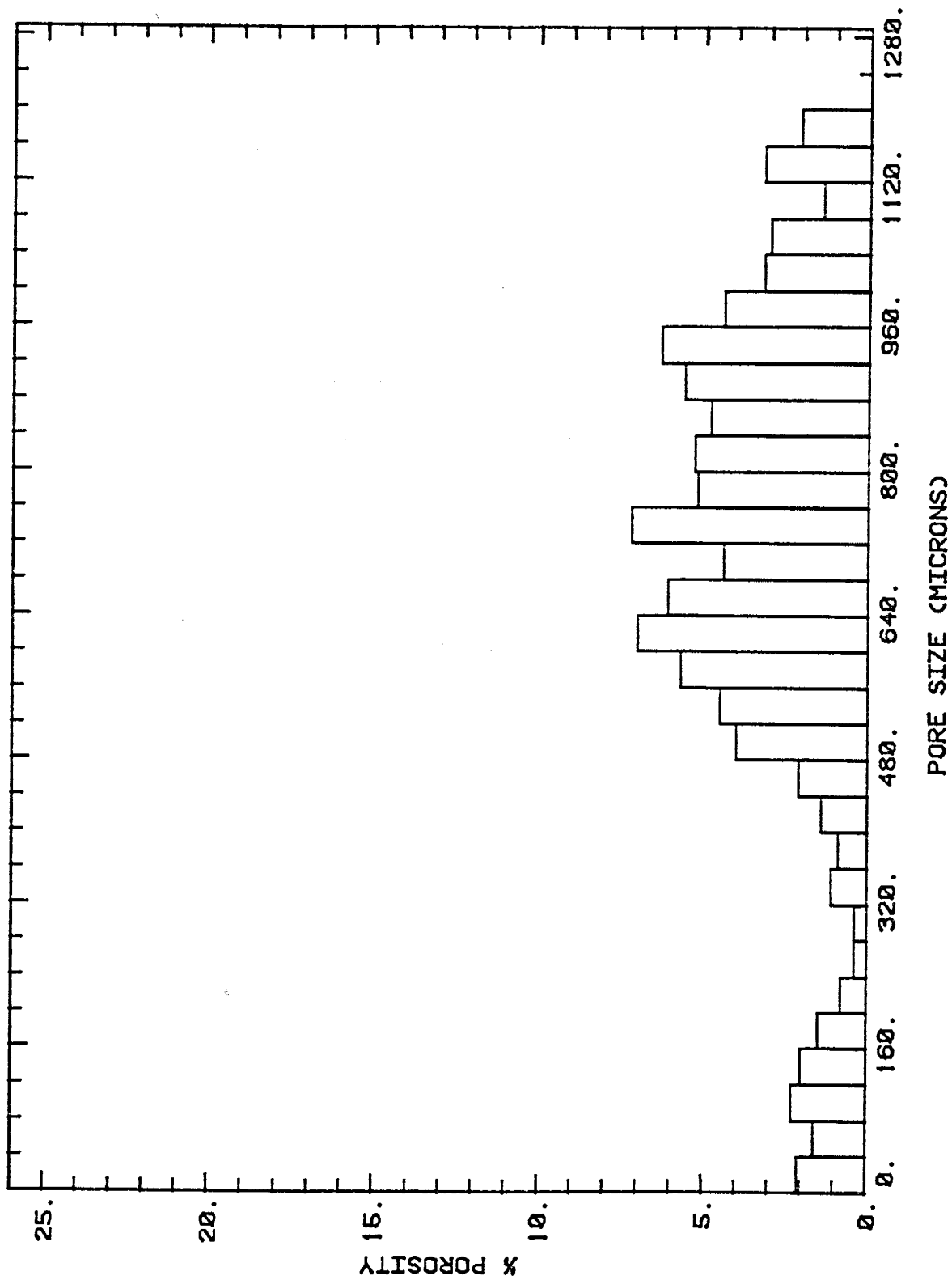


Fig. 4.20 Distribution of Pore Body Sizes for SA0

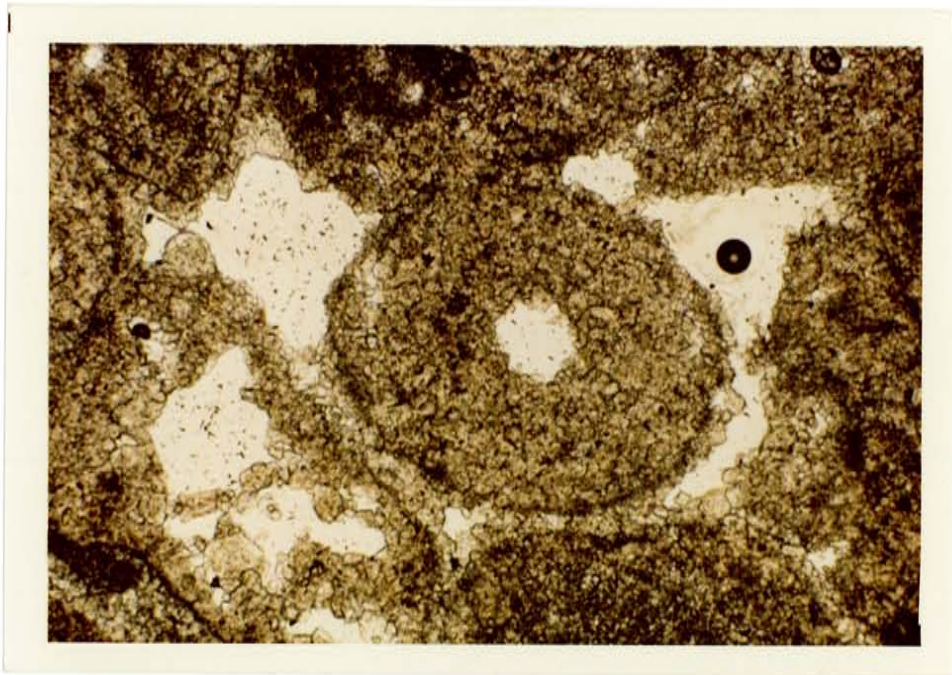


Fig. 4.21 Photomicrograph of SAO
Pores are colored white.
Magnification: 50x

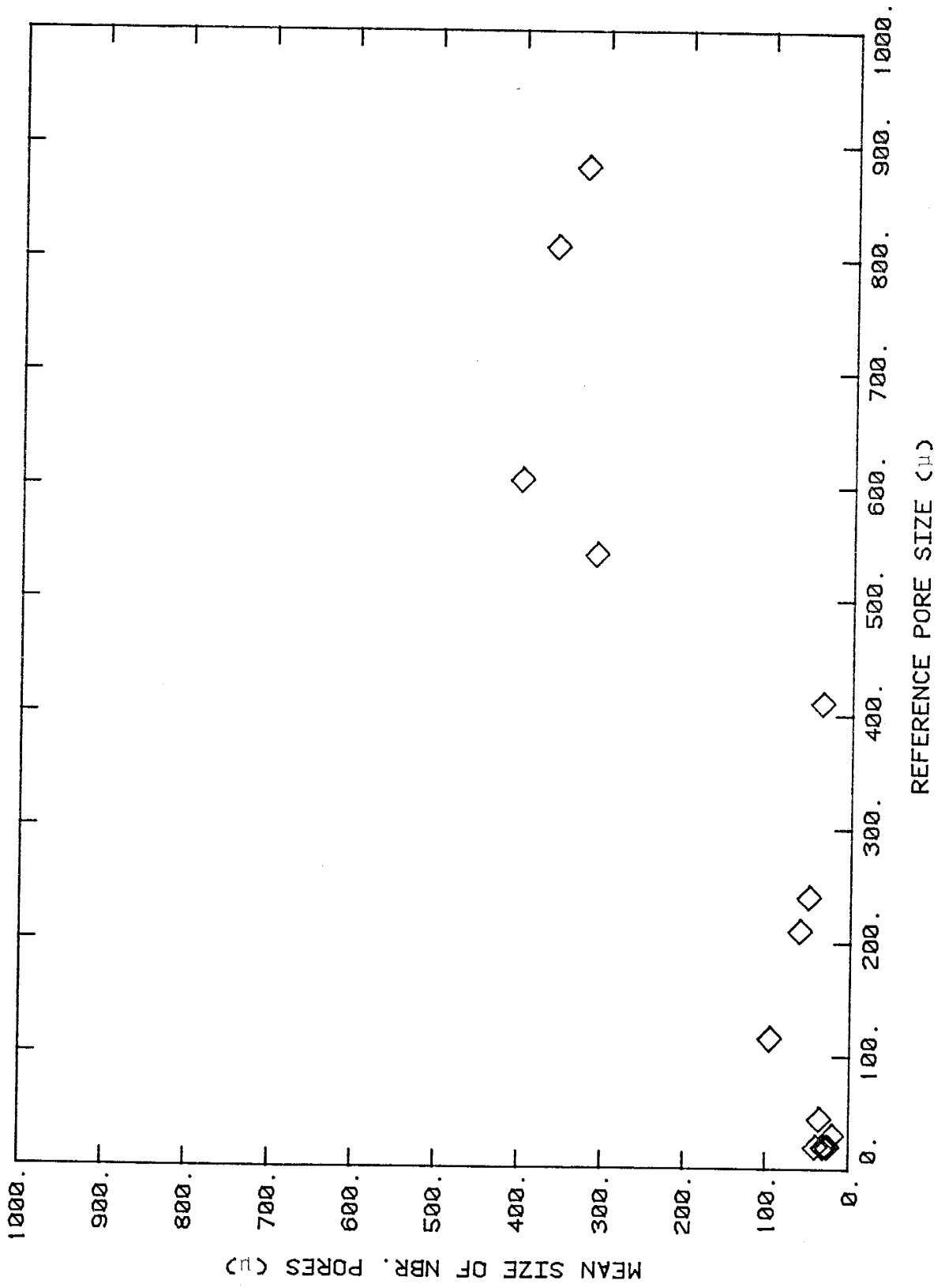


Fig. 4.22 Spatial Distribution of Pores in SA0

micropores which control fluid movement to and from the center of the grain. The spatial pore distribution data for SAO are weakly ($r^2 = 0.69$) correlated, which suggests that preferential flow paths may exist. Reference pores up to about 0.5 mm appear to be proximal primarily to micropores. Larger intergranular pores tend to be associated with pores of like size; thus, they may act as preferential flow conduits.

The arrangement of pores in sample SAO is very similar to the system idealized by the Coats-Smith model. A pore system composed of large, solution-enhanced channels which connect to isolated oomoldic pores only through intercrystalline micropores may well be a physical representation of DEPV.

The pore structure of core M1 (Figs. 4.23 - 4.27) is the most heterogeneous of all of the samples. The rock is composed of tightly woven euhedral to anhedral dolomite crystals. Seventeen percent of the pore space consists of intercrystalline pores of less than 25 microns. Large vugs directly connected by fractures and stylolites (pressure solution seams) dwarf the surrounding micropores (Fig. 4.27). These connected megapores may well function as preferential flowpaths in miscible displacements. The spatial distribution of pores shown in Figure 4.28 supports this idea. There is essentially a linear relationship ($r^2 = 0.95$) between the sizes of reference pores and neighboring pores. Micropores are connected primarily to each other,

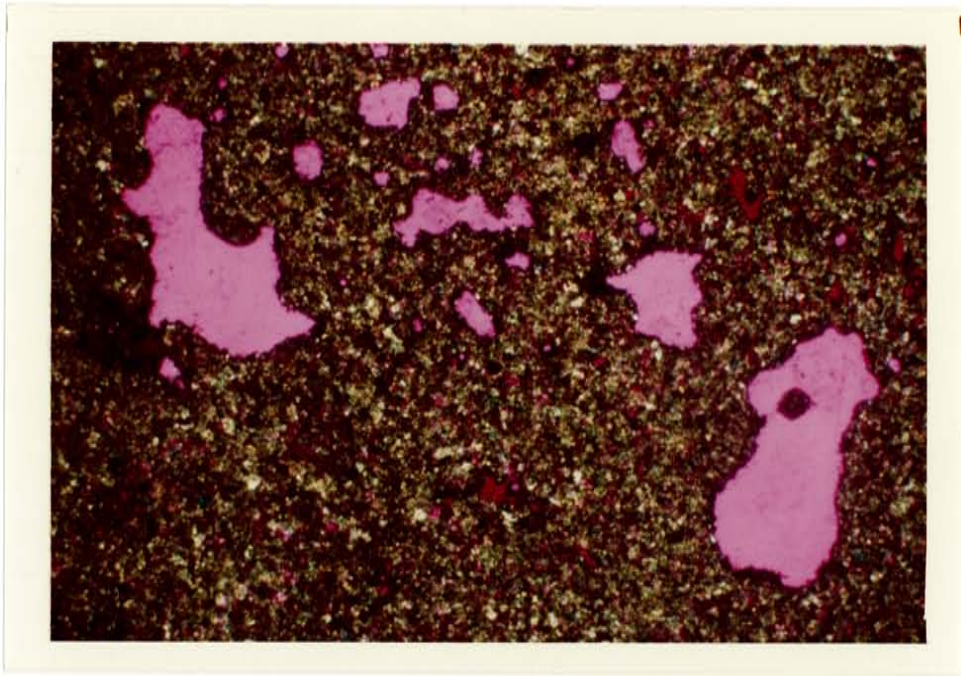


Fig. 4.23 Photomicrograph of M1
Pores are colored pink/purple.
Magnification: 50x

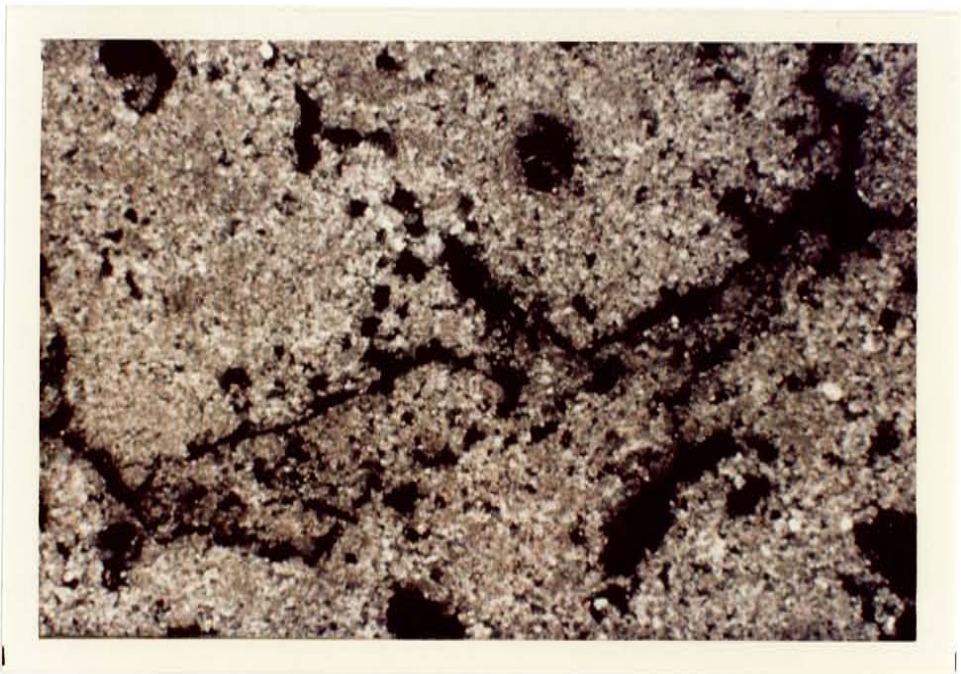


Fig. 4.24 Photomicrograph of M1
Pores are colored black.
Magnification: 50x

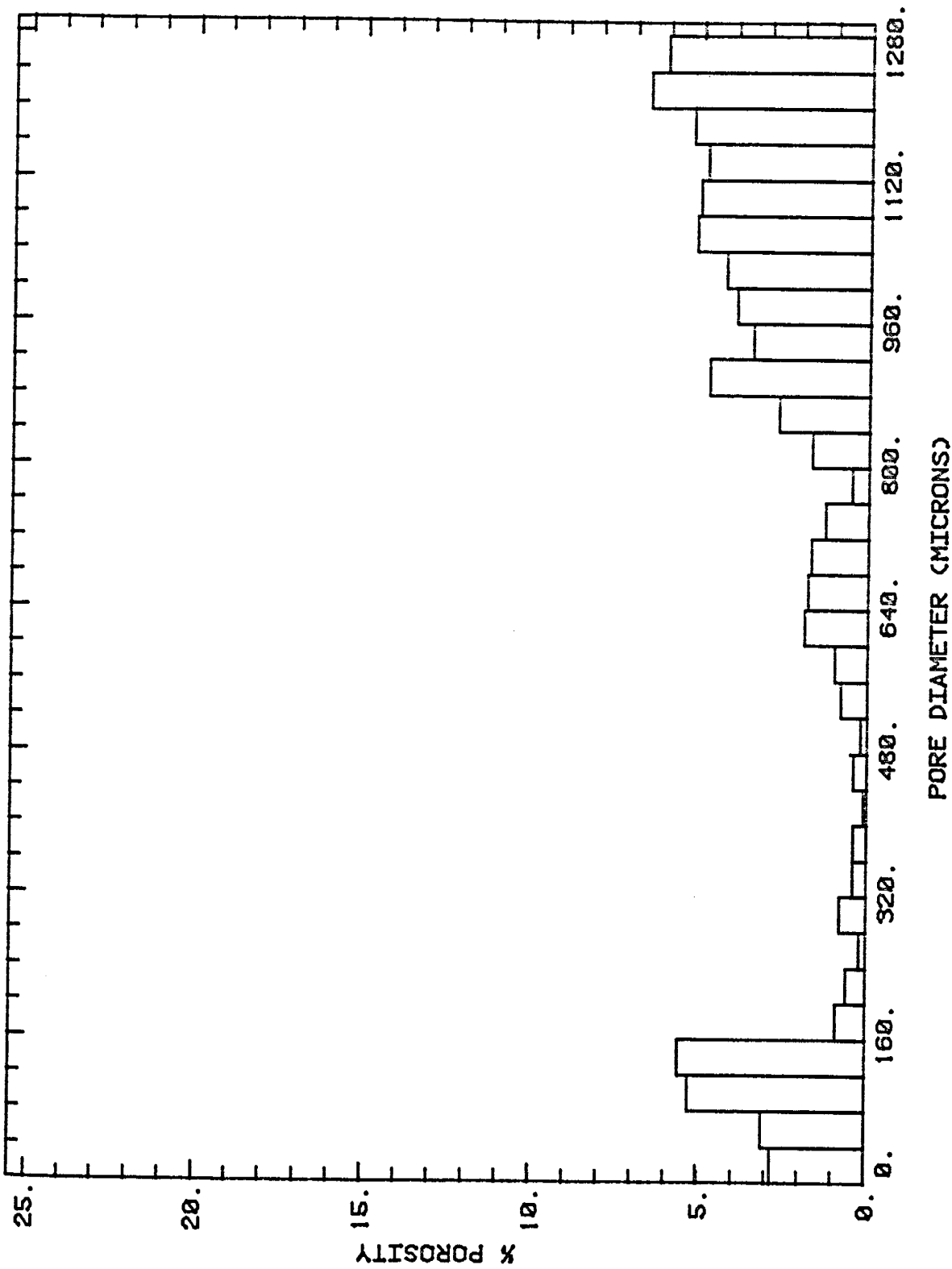


Fig. 4.25 Distribution of Pore Body Sizes for the Lower 84% of Porosity in M1

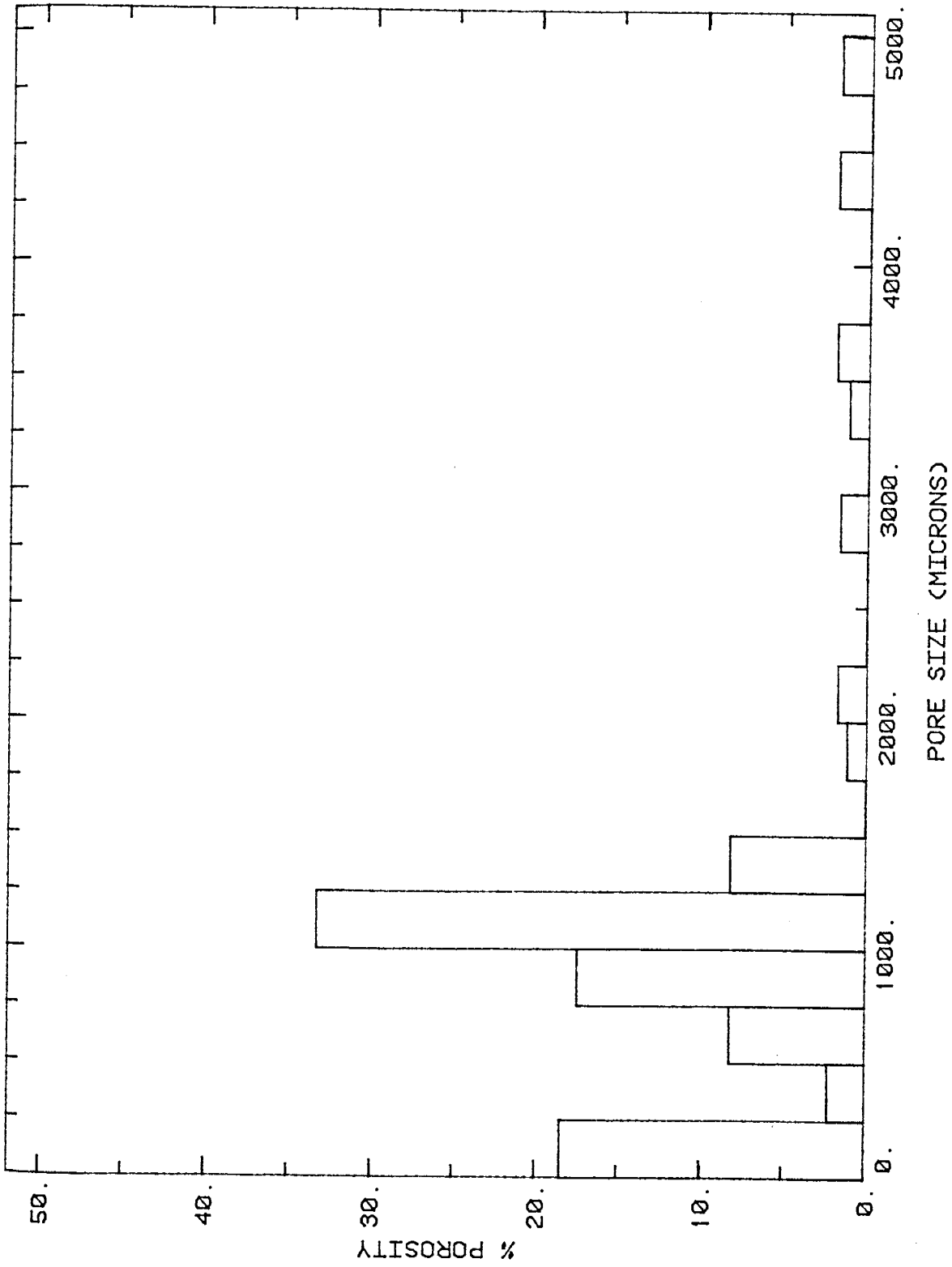


Fig. 4.26 Distribution of Pore Body Sizes for M1

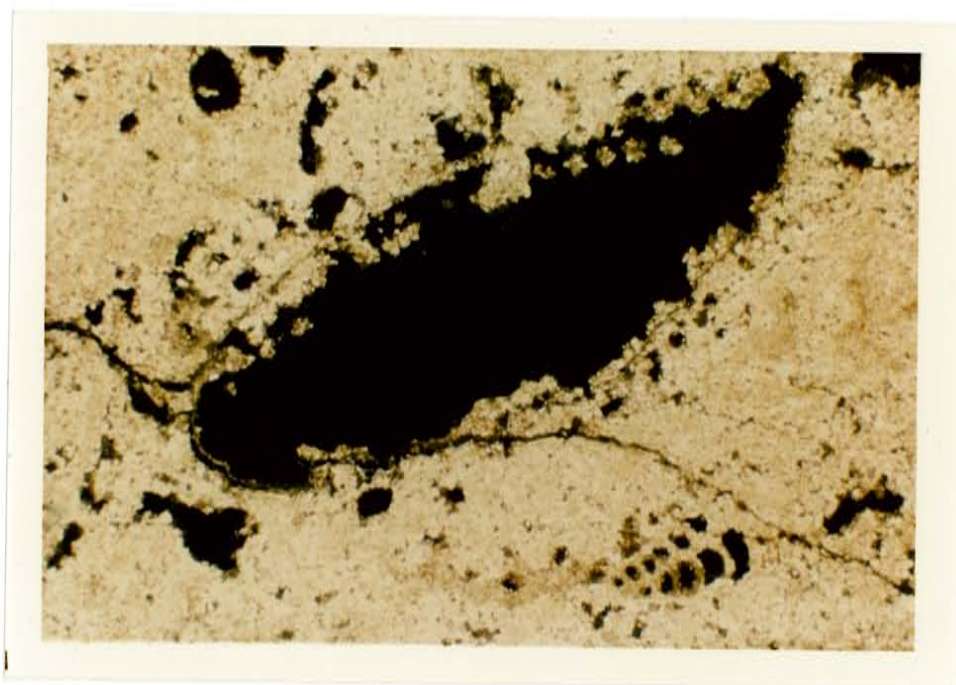


Fig. 4.27 Photomicrograph of M1

Pores are colored black.

Magnification: 25x

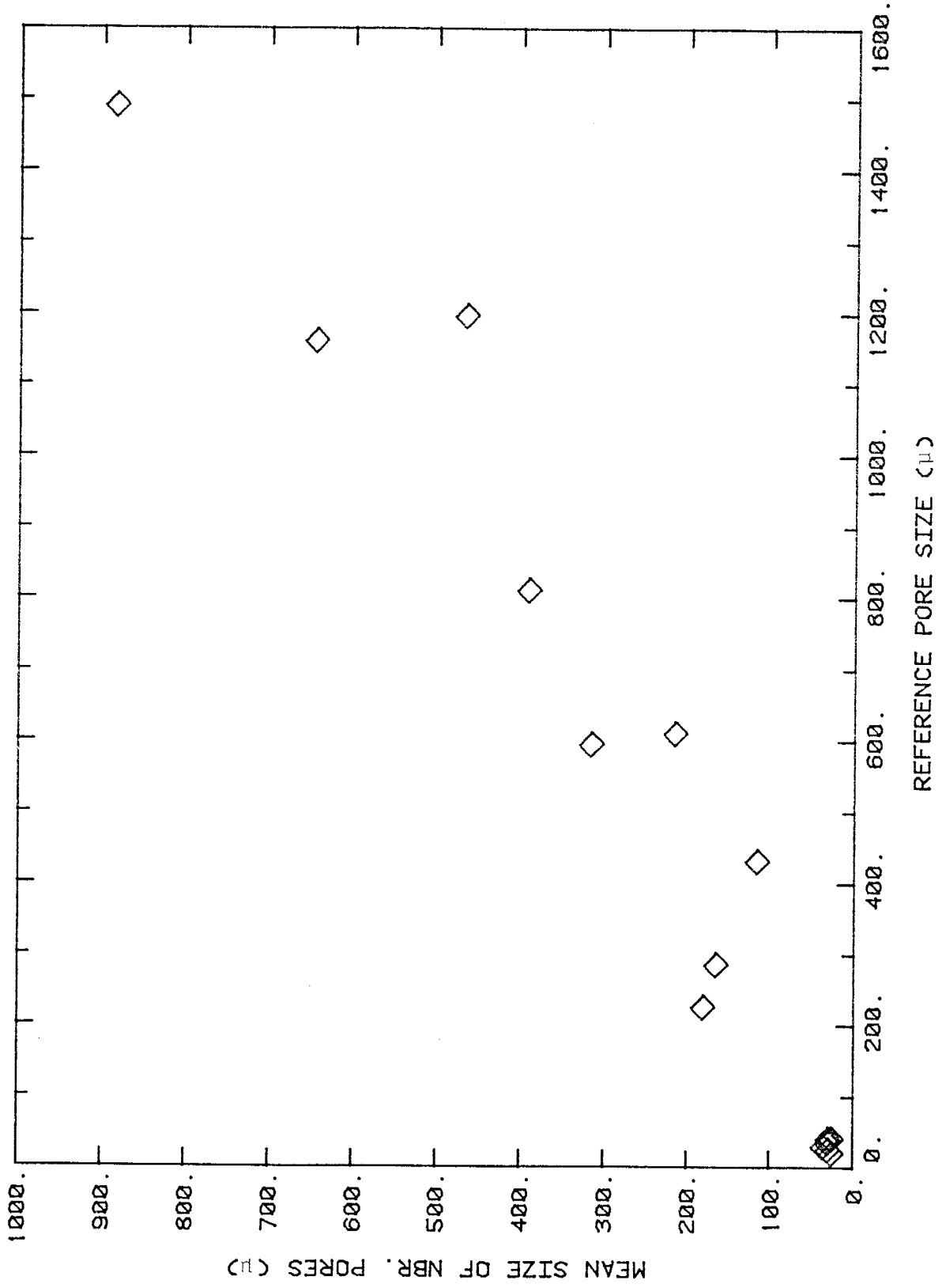


Fig. 4.28 Spatial Distribution of Pores in MI

while larger vugs and solution-enhanced fractures are connected to voids of similar size.

CHAPTER 5
RELATION OF PORE STRUCTURE
OBSERVATIONS TO DISPLACEMENT RESULTS

In the discussion which follows, data gathered from single-phase displacements in seven rock cores are related to pore system structure. Results of the displacements are summarized in Table 5.1. Properties of the studied sandstone and carbonate core samples are summarized in Appendix A, Table A.1.

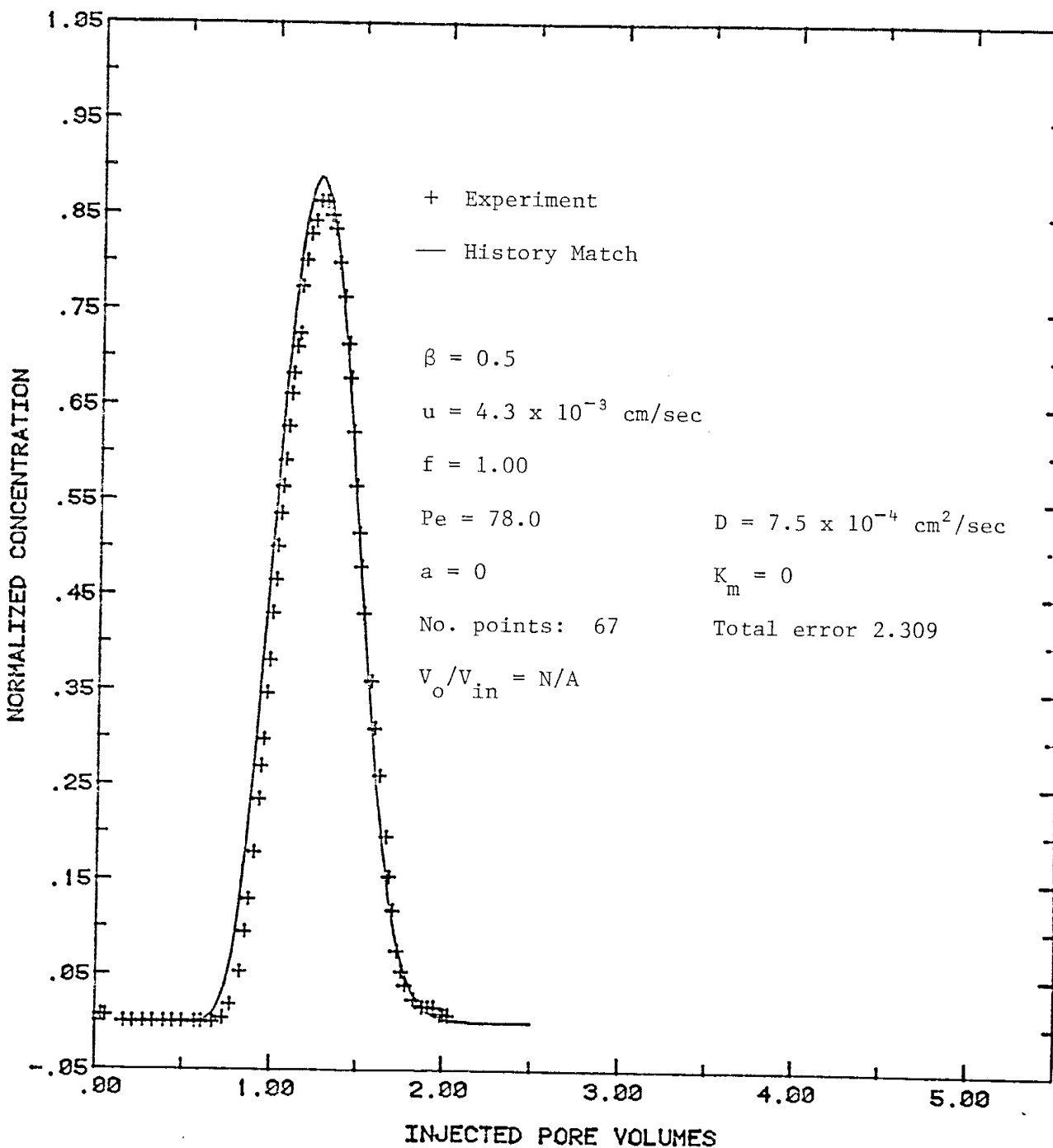
Sandstone Cores

Results of typical, nominal 10 ft/day displacements in samples B1, F2 and R1 are shown in Figures 5.1 - 5.3. Values for Coats-Smith model parameters are shown on the plots, along with other information related to displacements. Additional displacements in these sandstone cores, not reported herein, were performed at varied flow rates; differences of results between displacements were minimal (Orr and Taber, 1984).

For cores B1 and F2, the effluent composition curves are symmetric about one pore-volume-injected. Both displacements are adequately modeled by a Peclet number alone; mass transfer in F2 was almost immeasurable and in B1 was non-existent. Core B1 contains a relatively uniform pore system which is, at least qualitatively, similar to that described in Figure 2.2b. Core F2 differs from B1

TABLE 5.1 Summary of Miscible Displacement Results (after Orr and Taber, 1984)

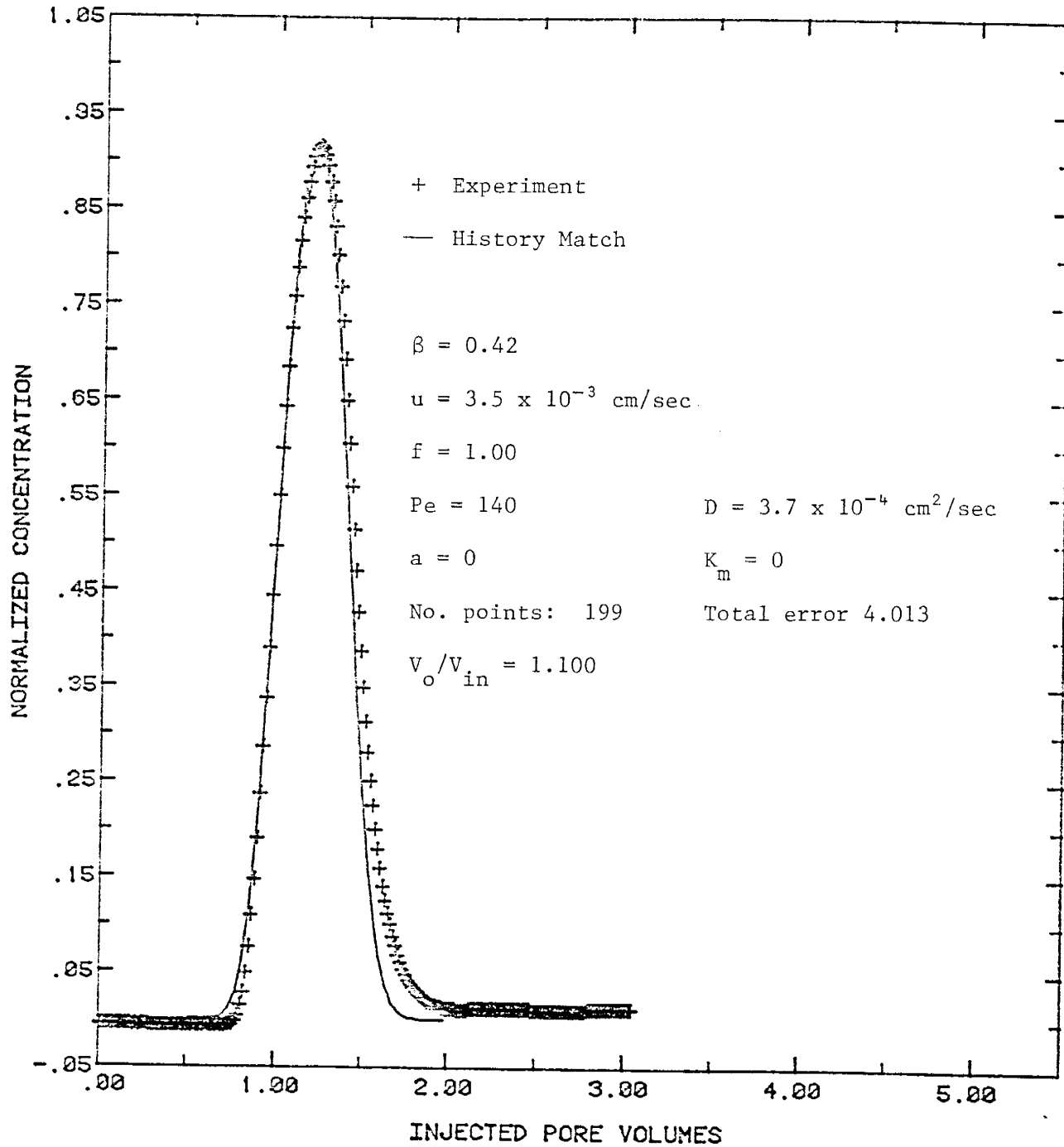
Exp't. No.	Core	Average Interstitial Velocity cm/sec	Pulse Size, Pore Volumes	Flowing Fraction	Peclet No. $\frac{uL}{D}$	Dispersion Coefficient cm^2/sec	Damköhler No. $\frac{KL}{m \cdot u}$	Mass Transfer Coefficient sec^{-1}
9	B1	4.3×10^{-3}	0.5	1.0	78	7.5×10^{-4}	0	0
17	F2	3.5×10^{-3}	0.42	1.0	140	3.7×10^{-4}	0	0
20	R1	3.5×10^{-3}	0.503	0.982	236	3.2×10^{-4}	0.076	1.2×10^{-5}
31	WW2	2.8×10^{-3}	0.51	0.897	27.8	1.4×10^{-3}	$<10^{-4}$	$<10^{-7}$
22	H1	4.4×10^{-3}	0.42	0.687	14.1	5.1×10^{-3}	0.192	5.2×10^{-5}
37	SA0	2.5×10^{-3}	--	0.771	21.7	7.8×10^{-3}	0.395	1.5×10^{-5}
34	M1	2.5×10^{-3}	0.34	0.621	6.5	1.2×10^{-2}	0.117	9.2×10^{-6}



Experiment No. 9
 Length: 13.6 cm
 Pore Volume: 28.6 cm³
 Air permeability: 180 md
 Fluids: C_{10}/C_{11}
 Dead volume: 0.40 cm³

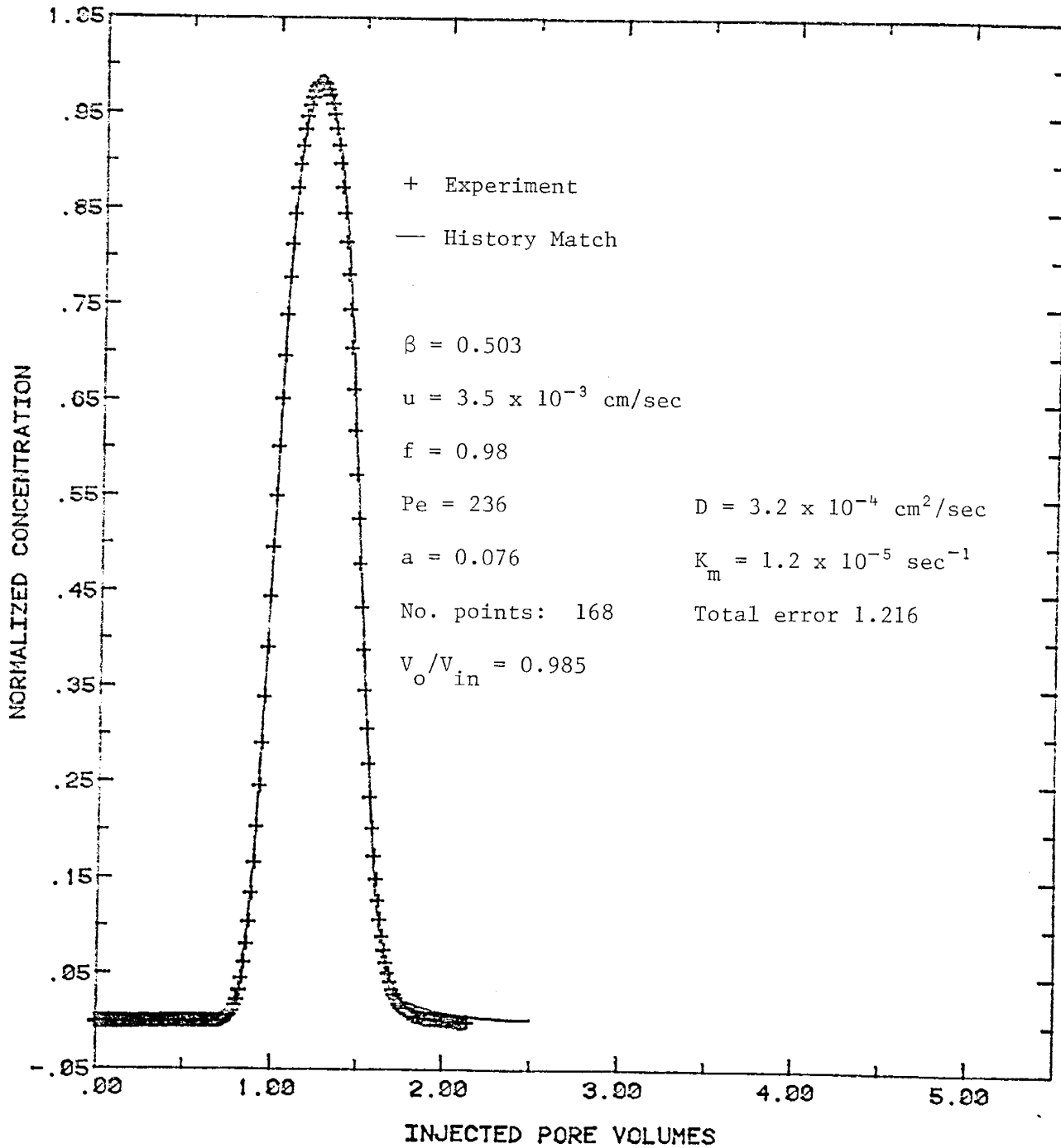
Core: B1
 Diameter: 3.81 cm
 Porosity: 18.2%

Fig. 5.1 Effluent Composition Curve for B1



Experiment No. 17	Core: F2
Length: 14.92 cm	Diameter: 3.81 cm
Pore volume: 34.17 cm ³	Porosity: 20.1%
Air permeability: 380 md	
Fluids: 0.4%/0.52% sucrose in Cl ⁻ brine	
Dead volume: 1.1 cm ³	

Fig. 5.2 Effluent Composition Curve for F2



Experiment No. 20
 Length: 21.8 cm
 Pore volume: 10.55 cm³
 Air permeability: N/A
 Fluids: 0.4%/0.52% sucrose in Cl⁻ brine
 Dead volume: 0.365 cm³

Core: R1
 Diameter: 1.59 cm
 Porosity: 24.5%

Fig. 5.3 Effluent Composition Curve for R1

primarily in grain size; F2 has smaller grains, and therefore smaller pores than does B1. Also, the Berea material contains more clay and carbonate precipitates than the Frannie core, which may explain the larger dispersion coefficient of B1 compared to that of F2. The Frannie, then, appears to be similar to the idealized system in Figure 2.2a. Both of these dispersion coefficients, along with the value obtained for sample R1, are considered to be low relative to those recorded for the carbonate rocks. Spatial pore distribution data for B1 and F2 are very similar, and by their randomness suggest that no preferential flow is likely in those samples.

In contrast to the preceding sandstones, results of a displacement in the Rock Creek core (R1) produced a flowing fraction of slightly less than one and a measurable mass transfer coefficient. Table 5.2 gives a summary of pore structure observations and displacement results. Sample R1 exhibits a wider distribution of pore sizes compared to the other sandstone cores. Large (~500-640 microns), secondary pores resulting from grain dissolution are non-uniformly distributed in the core; these sparse pores may act as preferential flow paths, if only in a minor way. Of the three sandstone cores examined, only the Rock Creek sample produced a measurable mass transfer coefficient. This indication of restricted pore space is probably related to the distribution of clay matrix in the rock. The restricted pores may occur as medium-sized voids which are surrounded

Table 5.2 Summary of Pore Space Data

Sample	Pore Size Distribution		Non-Random Permeability Barriers	Preferential Flow Paths	Pore Type	Exp't. No.	F	D cm ² /sec	K _m sec ⁻¹
	# Modes	Mean ±Std. Dev. (µm)							
Berea SS (B1)	One	169.44 ± 83.24	None	None	G	9	1.0	7.5 x 10 ⁻⁴	0
Frannie SS (F2)	One	108.48 ± 62.98	None	None	G	17	1.0	3.7 x 10 ⁻⁴	<10 ⁻⁷
Rock Creek SS (R1)	One	259.80 ±165.62	Clay mineral pods (matrix)	Flow through type-G pores around clay pods	G	20	0.982	3.2 x 10 ⁻⁴	1.2 x 10 ⁻⁵
Wasson DM (WW2)	One	343.23 ±129.42	Minor anhydrite plugging	None	SC	31	0.897	1.4 x 10 ⁻³	<10 ⁻⁷
Seminole DM (H1)	Three	129.55 ± 90.95 500.00 ± 33.81 786.19 ±117.19	Anhydrite plugging	Flow through vugs indirectly connected by type-C pores	SC,V	22	0.687	5.1 x 10 ⁻³	5.2 x 10 ⁻⁵
San Andres FM (SAO) DM	Two	110.74 ± 66.60 769.84 ±200.81	Type-C pores arranged in spherical clusters	Flow through well-coordinated type-SC and type-V pores	SC,V,M, C	37	0.771	7.8 x 10 ⁻³	1.5 x 10 ⁻⁵
Maljamar DM (M1)	Many	Widest distribution of sizes	Preponderance of type-C pores, anhydrite plugging	Flow through fracture/stylolite-connected vugs	C,V,SF M	34	0.621	1.2 x 10 ⁻²	9.2 x 10 ⁻⁶

Lithologic Key:

SS = Sandstone
DM = Dolomite

Key to Pore Types:

C = Inter-crystalline <25µm
F = Fracture/Stylolite
G = Intergranular
M = Moldic
S = Solution Enhanced (Prefix)
V = Vugular

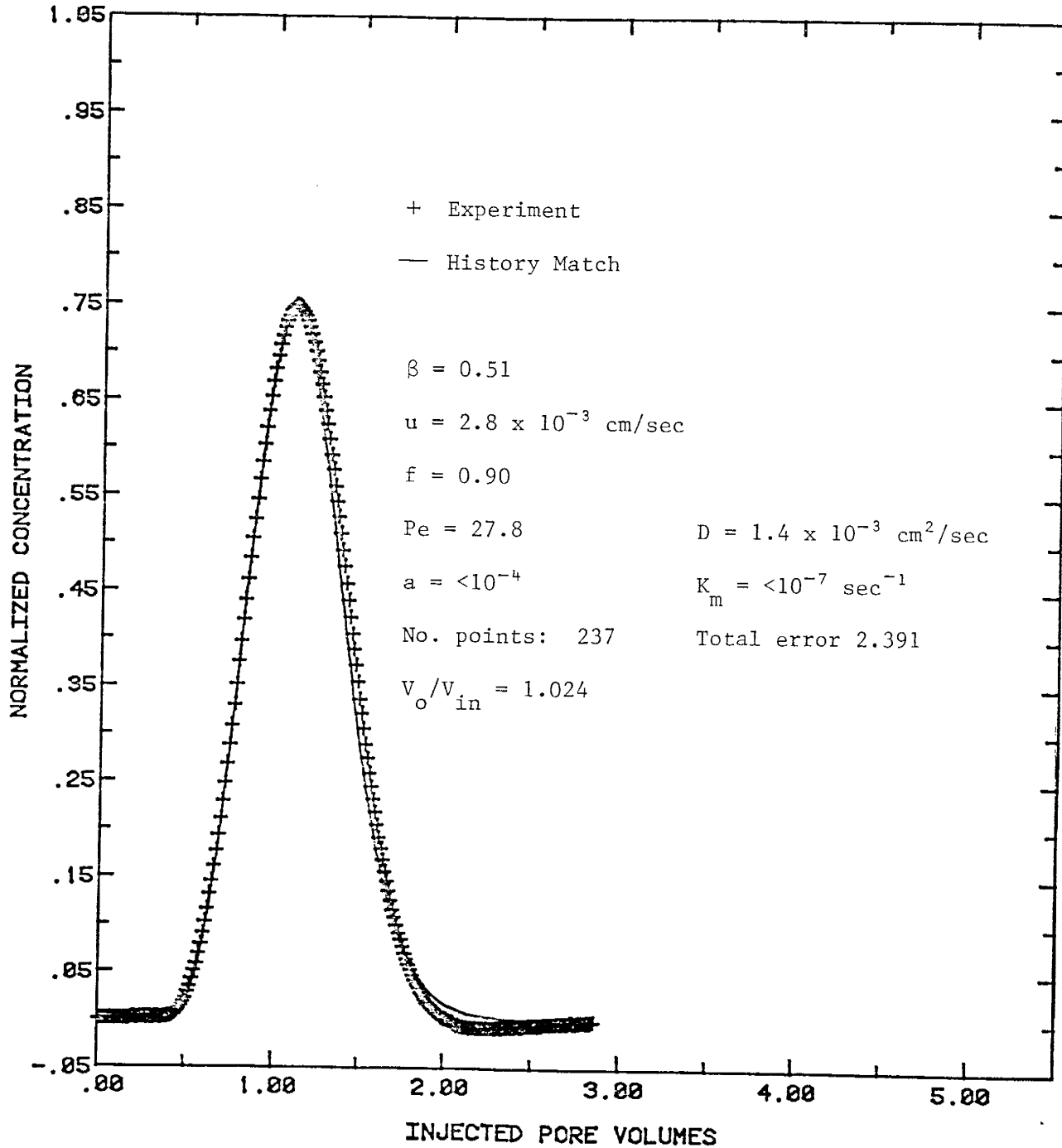
by clay pods, interstices in the clay, or more likely, both.

Preferential flow may be the reason for the flowing fraction value of less than one (0.982) for this core; this is supported by the weak linear trend in the spatial pore distribution data (Fig. 4.11). Another possible explanation is error in the measurement of f . Small pump rate deviations, for example, could affect the arrival time of the fluid pulse, which would directly translate into error in the flowing fraction value (Orr and Taber, 1984). Though the effect of pore structure heterogeneity on flowing fraction in core R1 is in question, the measurable mass transfer coefficient suggests the existence of restricted flow.

To summarize, the displacement results for the sandstones are characterized by flowing fractions at or near one and low or non-existent mass transfer coefficients. Dispersion varies between samples, but, in general, sandstones exhibit smaller transition mixing zones than do the carbonates studied. High flowing fractions are associated with narrow, uniform pore size distributions and well-connected, relatively unrestricted flow paths.

Carbonate Cores

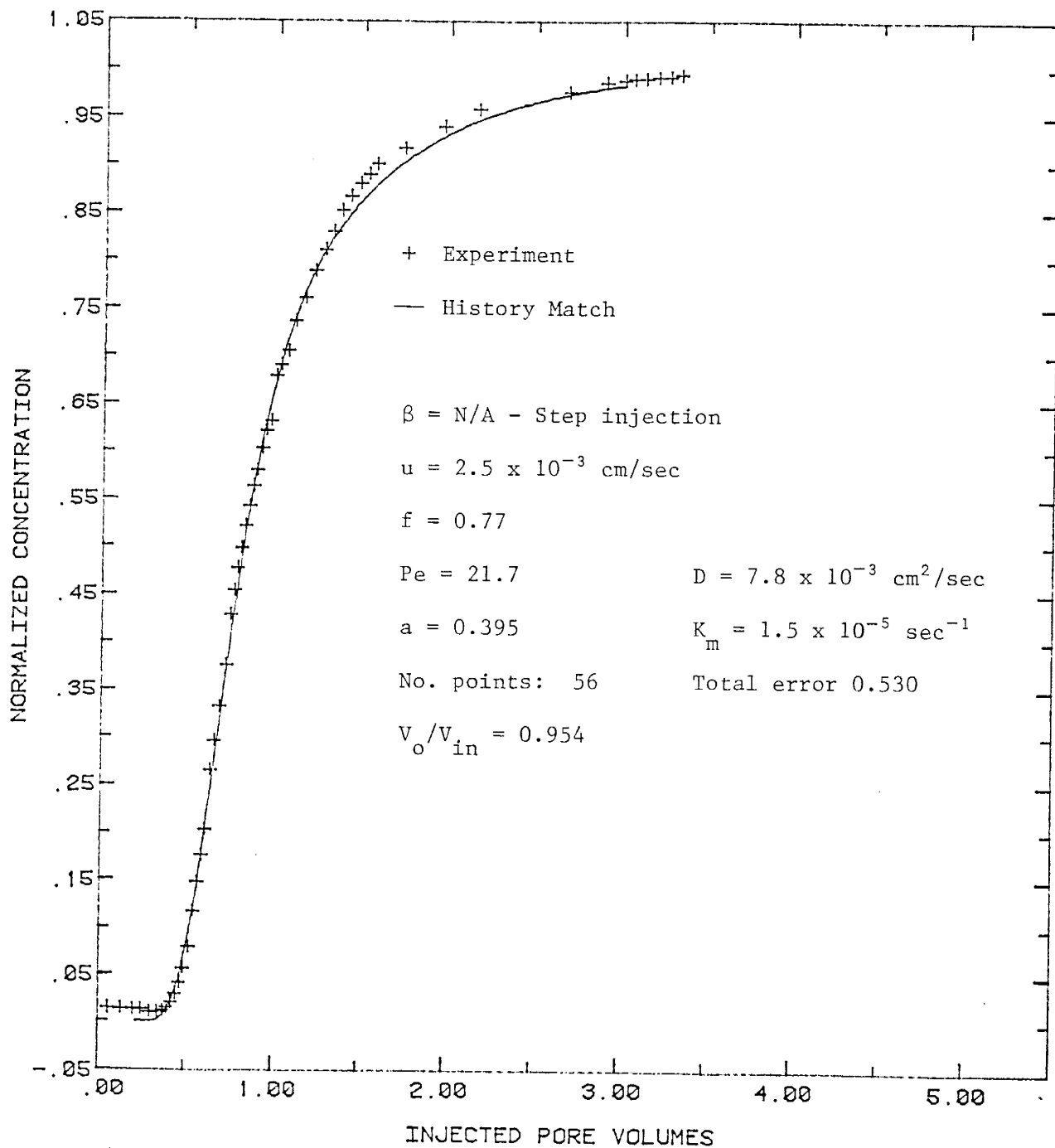
Results of displacements in carbonate cores WW2, SAO, H1 and M1 are presented in Figures 5.4 - 5.7. The carbonate cores exhibited greater variation in both displacement results and pore structure than did the sandstones.



Experiment No. 31
 Length: 13.7 cm
 Pore volume: 3.70 cm³
 Air permeability: 90 md
 Fluids: C_{10}/C_{11}
 Dead volume: 0.575 cm³

Core: WW2
 Diameter: 1.27 cm
 Porosity: 21.3%

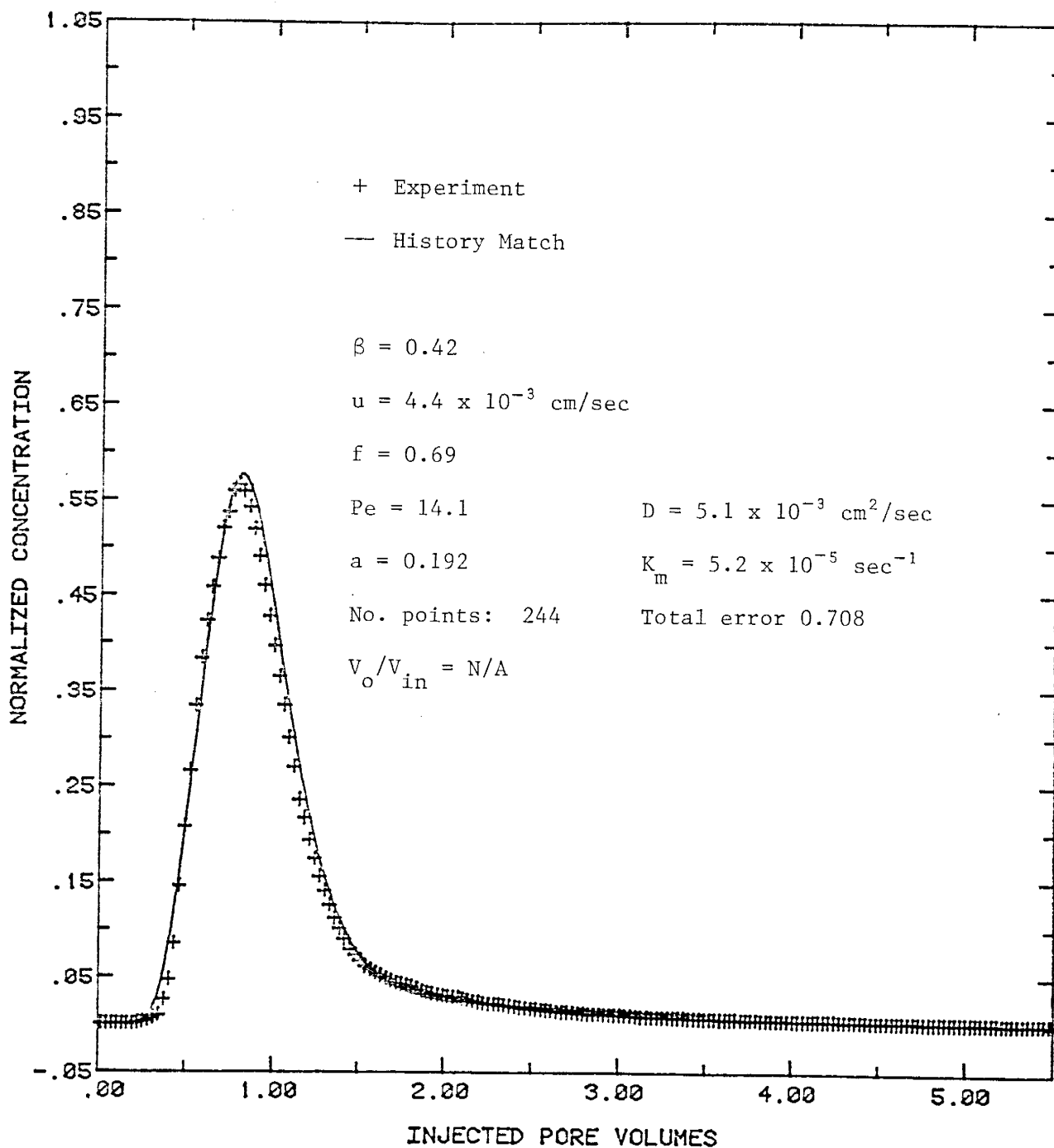
Fig. 5.4 Effluent Composition Curve for WW2



Experiment No. 37
 Length: 66.7 cm
 Pore volume: 235.16 cm³
 Air permeability: 124 md
 Fluids: ethylbenzene/ethylbutyrate
 Dead volume: 1.262 cm³

Core: SA0
 Diameter: 3.81 cm
 Porosity: 17.4%

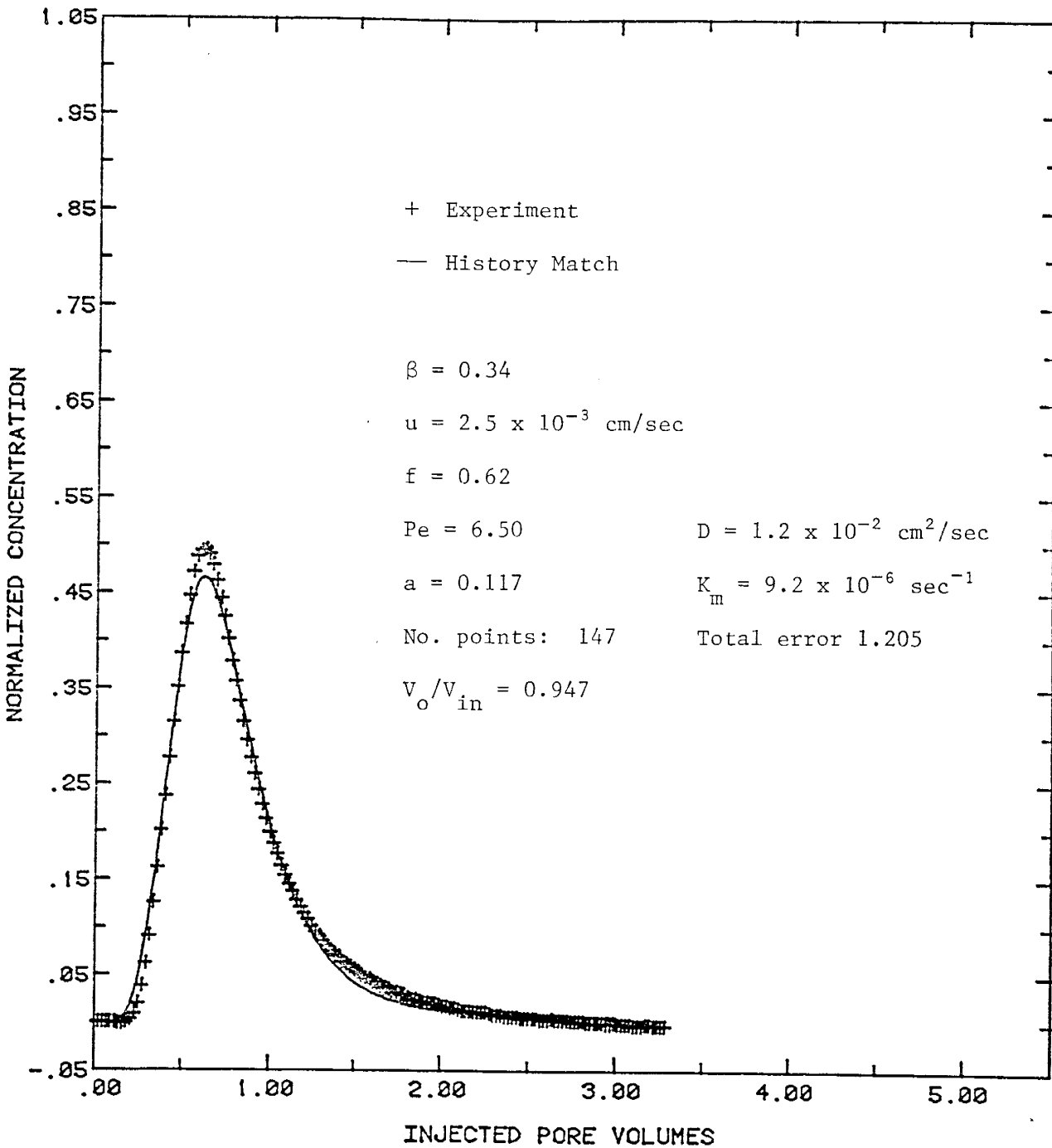
Fig. 5.5 Effluent Composition Curve for SA0



Experiment No. 22
 Length: 16.2 cm
 Pore volume: 33.7 cm³
 Air permeability: 40 md
 Fluids: ethylbenzene/ethylbutyrate
 Dead volume: N/A

Core: H1
 Diameter: 3.81 cm
 Porosity: 18.2%

Fig. 5.6 Effluent Composition Curve for H1



Experiment No. 34	Core: M1
Length: 31.5 cm	Diameter: 1.39 cm
Pore volume: 5.67 cm ³	Porosity: 9.1%
Air permeability: 6 md	
Fluids: 0.4%/0.52% sucrose in Cl ⁻ brine	
Dead volume: 0.358 cm ³	

Fig. 5.7 Effluent Composition Curve for M1

Figures 4.12 and 4.13 show a photomicrograph and the pore size distribution, respectively, of sample WW2. The distribution of pore sizes was not greatly different from that of the Rock Creek core, as the average pore size and standard deviation data in Table 5.2 indicate. Typical pore geometry of the 200-400 micron-sized voids in WW2 is spherical to ovate, a function of the diagenesis of the rock. No clays were detected in this nor in any other of the carbonate cores studied. A minor quantity of anhydrite precipitate is present in pores greater than 200 microns in size, and occurs as slender, interlocking crystals with patchy distribution. By comparison, the anhydrite in WW2 is distributed less uniformly and sparsely than is dolomite precipitate in the Berea sand, but more so than cements in carbonate samples H1 and M1.

Displacement results (Fig. 5.4) show a flowing fraction lower than, but still comparable to, those of the sandstones. The restricted pore volume ($1-f$, or 10.3%) is probably related to the distribution of anhydrite cement in the pores. The role of mass transfer is minimal in this core, so it is unlikely that true preferential flow paths exist; rather, the anhydrite probably forces the fluids to seek somewhat less direct paths to the core outlet, resulting in a broader transition zone. This idea is supported by the dispersion coefficient (1.4×10^{-3} cm²/sec), which is an order of magnitude greater than that recorded for any of the sandstones. The spatial

distribution of pores (Fig. 4.14) also supports this idea; the data are weakly ($r^2 = 0.59$) if at all correlated, which suggests that preferential flow does not occur.

The nature of pore coordination provides another possible explanation for the elevated dispersion coefficient. Qualitative observation of pore connectivity in thin section suggests that micropores may occur in sufficient quantity, in critical areas, to cause a greater fluid residence time, and hence greater opportunity for mixing. Since pores of all sizes appear to be well-connected, no stagnant pore volume exists, so no mass transfer occurs; the preponderance of micropores may simply slow down the flow and allow more time to mix fluid concentrations within pores.

The pore size distribution and photomicrographs of the San Andres Formation outcrop core (SAO) are shown in Figures 4.19 - 4.21. Figures 4.15 - 4.17 give similar data and photos of reservoir core H1. Both samples show much broader distributions of pore sizes than the WW2 core or the sandstones. Displacement results for outcrop sample SAO (Fig. 5.5) show a low flowing fraction (0.771), a high dispersion coefficient and a measureable mass transfer coefficient, all of which translate into an asymmetrical effluent composition curve, early appearance of the 50% effluent concentration point, and a tailing effect on the curve due to the slow removal of fluids from restricted pores.

Such results are typical of the more heterogeneous carbonate cores (SAO, H1 and M1). The data (Figs. 5.5 - 5.7) indicate the existence of preferential flow paths through which fluids move at higher velocities than in the restricted pore fraction $(1-f)$. Thin section observations of pore structure in SAO support this interpretation. Preservation of the primary granular fabric in the core, coupled with extensive solution-enhancement of the connectivity between interparticle pores has created a pore structure which contains wide flow channels around the spherical ooids. Oomoldic pores are present, and are connected to the wide channels only by means of low-permeability micropores. The micropores occur in cryptocrystalline dolomite which has replaced the grain walls. Presumably, fluid within oomoldic pores was exchanged with fluid in the preferential flow paths by diffusion. Diffusive exchange was much slower than flow in the wide channels; thus, pore structure in core SAO is similar to that of Figure 2.2c and closely approximates the system idealized in the Coats-Smith model.

Outcrop sample SAO and reservoir core H1 showed similar displacement behavior, but the structure of the pore systems in these two rocks is vastly different. In H1, extensive recrystallization occurred, resulting in obliteration of the primary granular fabric and creation of a hypidiotopic dolomite fabric primarily containing small pores, but also medium- and large-sized voids (Fig. 4.15). The larger pores appeared to be connected to each other by small zones of

micropores. Thus, it is conceivable that preferential flow paths could have existed. This is supported by the apparent trend of the spatial pore distribution data in Figure 4.18. These data indicate an association of like-sized pores in close proximity to each other; hence, the possible existence of preferential flowpaths. Dispersion in the flowing stream was probably elevated by the presence of anhydrite cement in selected pores greater than 200 microns in size and in adjacent micropores. Flow in the plentiful micropores must have been slower, especially when the effects of the anhydrite are considered.

Thin sections of dolomite sample M1 exhibited the widest pore size distribution of the cores examined in this study (Figs. 4.25 and 4.26). Pervasive dolomitization, dissolution of pore-filling sulfates, pressure solution and fracturing have combined to create large vugs which are directly connected by open fractures and stylolites. These vugs are surrounded by a multitude of low-permeability micropores which appear to control the overall permeability of the rock (permeability to air: 6 mD).

This pore system is similar to the idealization shown in Figure 2.2d, and is nicely modeled by a low flowing fraction, a high dispersion coefficient and a measureable mass transfer coefficient.

The flowing fraction (0.621) in M1 is the lowest such value recorded (Fig. 5.7) for all of the cores examined in this study. This value correlates well with the extremely

wide distribution of pore sizes in the sample, and with the strong linear trend ($r^2 = 0.95$) in the spatial pore distribution data (Fig. 4.28). Micropores are connected primarily to each other, and large voids are well-connected to like-sized pores. The vug-fracture system represents the main flowing stream through which fluids move at high velocities, while slower diffusive mixing occurs between restricted micropores and the flowing stream.

Summary of Results

Greater small-scale pore-structure heterogeneity occurs in the carbonates than in the sandstones studied. This heterogeneity, reflected in wide pore size distributions, is responsible for development of preferential flow paths with associated flowing fraction values significantly less than one, except in the case of the Wasson core. Dispersion coefficients are typically higher in the carbonates than in the sandstones. Mass transfer is more prevalent in the dolomites probably due to the preponderance of restricted pore volume in those samples.

Throughout this discussion, two aspects of small-scale heterogeneity have been considered. The first is the distribution of pore sizes. If the distribution is broad, early breakthrough of the displacing fluid may occur, but only if the pores are connected in ways which generate preferential flow paths. Fractures and solution pores

through fine matrix porosity, and no doubt other pore types, can generate such flow paths.

Discussion of Methodology

Qualitative observations of thin sections appear to be consistent with flow behavior in stable, single-phase miscible displacements in cores. Quantitative methods employed in this study produced varied results. The method used to determine pore size distributions produced explainable, consistent and reasonable results. An alternative method is to measure the area of a slice of a pore in the plane of the thin section. This is particularly useful when measuring pore sizes from a photomicrograph. Since a thin section is typically about 30 microns thick, some difficulty may be encountered in determining the bounds of a slice through a given pore. Consistency in measurement is critical, and it is recommended that only pore boundaries directly adjacent to the plane of the glass slide be measured.

The method used to determine spatial distributions of pores produced data which were at least consistent with qualitative observations of pore connectivity. A complimentary method of determining pore connectivity involves counting the actual number (coordination number) of pores which appear to be connected to a reference pore.

The vector analysis data proved highly variable, and could not be reasonably related to Coats-Smith model

parameters. It was hypothesized that a relation exists between dispersion coefficient (a reflection of the size of the transition zone) and mean flowpath orientation, as determined by vector analysis of pore structure in thin section. An inherent assumption here is that a mean flowpath normal to the direction of displacement would produce a higher dispersion coefficient than one resulting from a mean flowpath parallel to the longest axis of the core. Table 5.3 contains mean-flowpath-vector orientation ($\bar{\theta}$, relative to the displacement direction) and vector strength (\bar{r}_f) data for all of the studied cores. Results from the two data sets generated for each rock were inconsistent in most cases; this made interpretation of the data difficult. The inconsistency of the results created uncertainty about the accuracy and utility of the method. No relationship between mean flowpath vector strength in the direction of displacement and either dispersion coefficient or flowing fraction could be determined from the data plotted in Figures 5.8 and 5.9. There are strong doubts about the validity of the relationship between mean flowpath vectors and mixing behavior, so this method of pore space analysis is not recommended.

The physical validity of the Coats-Smith model itself needs to be examined. One of the problems in applying the model to natural porous media is the dependency of the model parameters on each other. For example, Orr and Taber (1984) report that flowing fractions near one result in insensitivity

TABLE 5.3 Summary of Flowpath Vector Analysis Data

<u>Sample</u>	<u>Set 1</u>		<u>Set 2</u>		<u>Average of Sets 1 & 2</u>	
	<u>$\bar{\theta}_1$</u>	<u>\bar{r}_{f1}</u>	<u>$\bar{\theta}_2$</u>	<u>\bar{r}_{f2}</u>	<u>$\bar{\theta}_c$</u>	<u>\bar{r}_{fc}</u>
B1	79.93°	0.06	71.94°	0.04	77.96°	0.05
F2	43.86°	0.20	62.17°	0.21	54.82°	0.21
R1	88.01°	0.01	24.51°	0.45	44.13°	0.29
WW2	67.74°	0.14	77.98°	0.10	74.13°	0.11
H1	104.08°	0.08	83.32°	0.04	92.67°	0.06
SA0	65.34°	0.12	14.19°	0.21	49.75°	0.16
M1	40.66°	0.05	57.65°	0.16	54.20°	0.09

Key to symbols:

$\bar{\theta}$ = mean flowpath orientation relative
to displacement direction (0°)

\bar{r}_f = strength of vector component in
the displacement direction

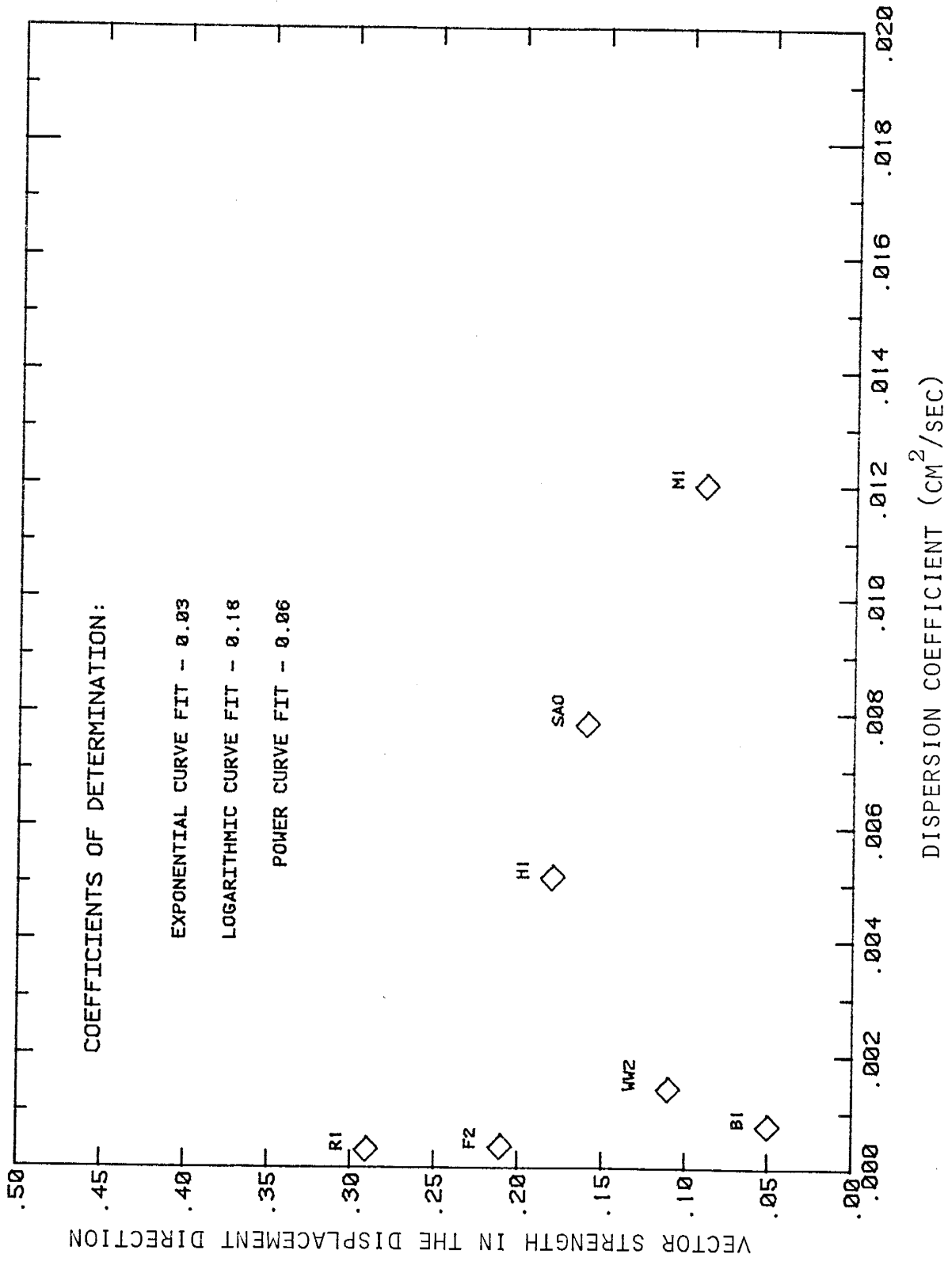


Fig. 5.8 Relation Between Flowpath Vector Strength and Dispersion

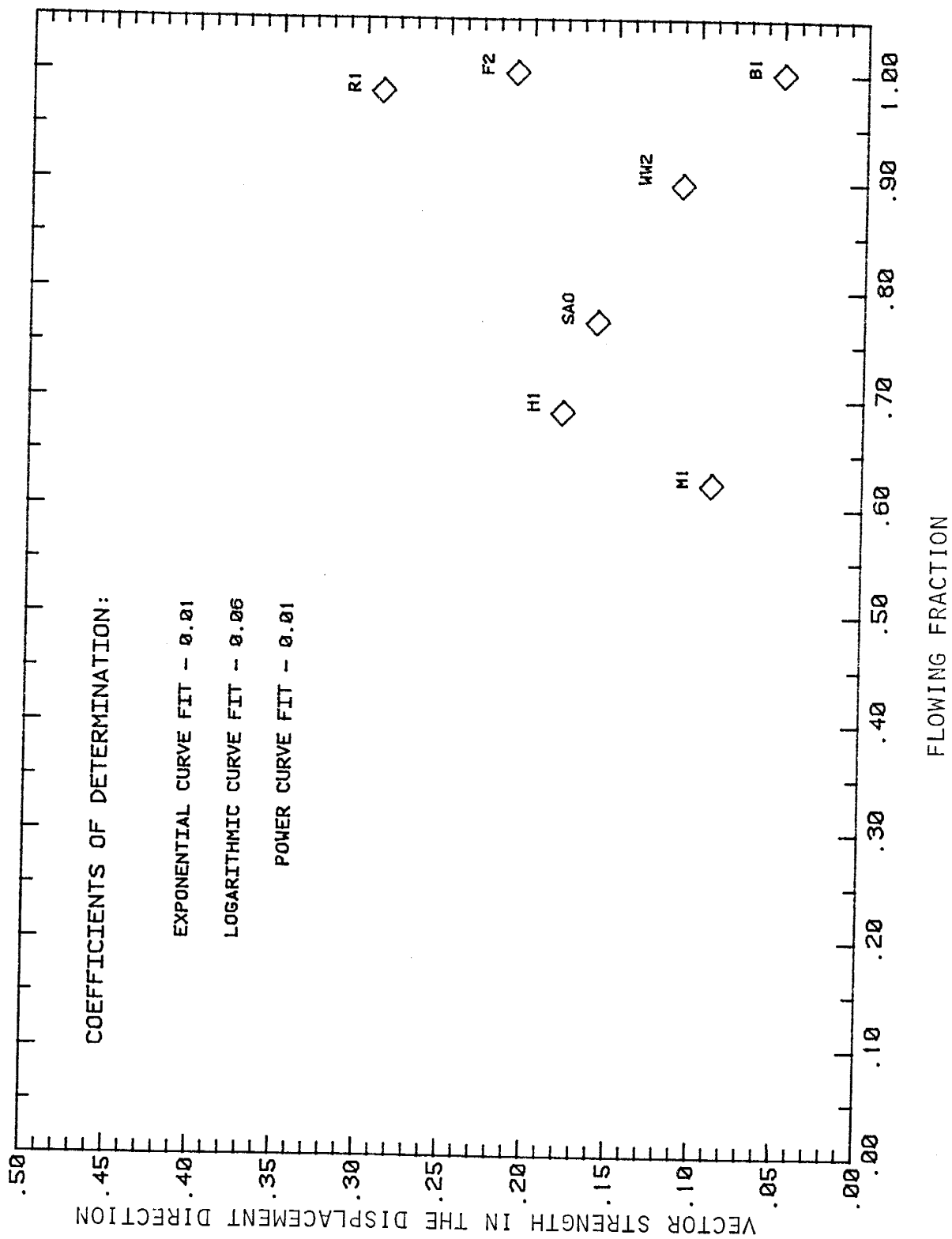


Fig. 5.9 Relation Between Flowpath Vector Strength and Flowing Fraction

of calculated effluent profile curve-fits to large variations in the value of the mass transfer coefficient. Stalkup (1970) and Batycky, et al. (1982), as cited by Orr and Taber (1984), point out that the effluent composition curves calculated for large mass transfer values are very similar to those obtained for small mass transfer values and large dispersion coefficients.

Another disadvantage of the model is that all forms of small-scale heterogeneity are indiscriminately lumped together and packaged as simple, finite parameters. Here, then, lies the fundamental problem in linking exacting mathematical flow models to highly variable core petrology which is difficult to describe in a consistent, quantitative fashion. In his conclusions concerning flow modeling, Heller (1963) stated this point well:

One should remember that fluid displacement includes some rather complex phenomena, and that ... (no) analytical approaches...can claim infallibility. In fact, in view of the incompleteness of the knowledge about many of the processes going on in porous media, it would probably be wise to regard model flow systems and numerical analysis as complementary rather than competing techniques for the prediction of reservoir displacement behavior.

Despite the inherent problems associated with modeling, the Coats-Smith model is, at least, a useful tool with which to describe displacement phenomena.

Questions of Scale

While questions remain about the physical validity of the Coats-Smith model, it is the only one in current use

which attempts to account for the effects of core heterogeneity on laboratory-scale displacements (Orr and Taber, 1984). A number of uncertainties in flow behavior at the reservoir scale have yet to be resolved. Questions about the impact of restricted pore volume on reservoir displacements have been addressed by Coats and Smith (1964), who argued that the dimensionless mass transfer group (a), which varies directly with porous-medium length, would be very large at the displacement length typical of reservoirs. A large mass transfer coefficient would be related to equalizations of fluid concentration between flowing and restricted volumes over a period of time which is short compared to the time required to flow an equivalent distance through preferential flow paths. Experimental results of long-core displacements by Stalkup (1970), Spence and Watkins (1980), and Batycky, et al. (1982) supported the conclusion that mass transfer rate limitations are less significant on a field scale (Orr and Taber, 1984). An assumption inherent in the reasoning of Coats and Smith (1964) is that dispersion and mass transfer coefficients are independent of displacement scale. This assumption is unlikely to be accurate for natural porous media. Heller (1963) pointed out that dispersion and mass transfer coefficients measured in rocks inevitably include averaged effects of small-scale heterogeneity; this idea is consistent with the fact that dispersion coefficients measured on field scales are often several orders of

magnitude greater than those measured on a laboratory scale (Orr and Taber, 1984).

Spence and Watkins (1980) extrapolated the Coats-Smith model parameters for a displacement in a heterogeneous, carbonate core to fit the greater times and distances associated with a reservoir flood. Their predicted effluent composition curve assumed the symmetrical appearance characteristic of a homogeneous pore system (Fig. 2.2a). A reasonable conclusion one might draw from this work is the expectation of an efficient displacement in a heterogeneous core as long as the length scale of the displacement is sufficiently great. The underlying assumption here is that, over interwell distances, only heterogeneity on the thin section scale is present in the reservoir. This is highly unlikely. Large-scale heterogeneity is common in petroleum-bearing formations, and includes lateral and vertical facies changes, variation in pay zone thickness, non-uniform reservoir geometries (i.e. coalescing shoestring sands), faulting and fracturing. The distribution of permeable zones may be non-random over the scale of the reservoir, possibly resulting in creation of large preferential flow paths through the field. Regional permeability may be controlled by the distributions of pore-filling cements, for example, or any other result of depositional and diagenetic processes. Thus, it is not at all clear what values of the Coats-Smith parameters might be appropriate at field scale.

There are, then, unresolved questions concerning the efficiency of field displacements, especially considering the added complexity of multiple phase interactions. Large-scale heterogeneity probably does influence reservoir floods, and detailed reservoir analysis must be done on an individual-field basis to assist in prediction of flood efficiency.

Future Work

Observation of pore structure in thin section is a useful means of examining the physical structure and configuration of pores and their relationship to displacement efficiency. One of the shortcomings of using real rocks in displacement experiments, though, is their variability. Virtually unlimited combinations of composition, shape, size, sorting and alteration of grains and cements in sandstones, for instance, can occur in reservoirs. The difficulty inherent with such variability in laboratory cores is the inability to isolate the effects of one petrophysical factor on mixing from those of others. It is suggested that displacements be run in very similar cores, with only one or two differences between them, so that any changes in displacement behavior may be associated with an individual physical characteristic. A large population of cores is recommended, as are multiple displacements in each core at varied flow rates, to ensure statistical validity of the results.

There are a number of questions about the effects of core handling procedures on pore structure which need to be examined, with the objective of improving and standardizing these procedures. Do the hydrocarbon extraction procedures performed on the cores prior to flooding alter or even remove constituents from rocks? What effects would such action have on pore structure? What are the effects of high-pressure flooding on delicate, authigenic clay minerals in sandstones? How much residence time is required for a sulfate-saturated brine to precipitate gypsum in a core? "Before-and-after" thin section and SEM examination, as well as permeability tests might give some indication of the extent of alteration, if any, which results from core handling procedures.

A simple experiment to investigate the effects of the averaging of pore-structure heterogeneity on Coats-Smith parameters could be conducted, by which cores of radically different pore structure are butted together to form one core. Coats-Smith parameters for separate displacements in a homogeneous sandstone and a heterogeneous carbonate, for example, would be determined, then the cores would be joined and a third displacement run. Comparison of the resulting parameters to those of the individual core floods might give some indication of the sensitivity of the dispersion and mass transfer coefficients to averaged pore structure.

CHAPTER 6

SUMMARY AND CONCLUSIONS

Results of seven single-phase miscible displacements are presented and are interpreted using the Coats-Smith model. Quantitative and qualitative observations of pore structure in thin section lead to the following conclusions:

1. The structure of pore systems in reservoir cores fundamentally influences displacement efficiency.
2. Small-scale heterogeneity of pore structure is responsible for mixing effects which result in early breakthrough of the displacing fluid and a flowing fraction less than one for displacements at the laboratory core scale.
3. A wide distribution of pore sizes is necessary but not in itself sufficient to produce a low flowing fraction. Also required are pore connections which result in the generation of preferential flow paths.
4. Flowing fraction values for the three sandstone cores were very close to one; pore structures in these rocks were much more homogeneous than those in most of the carbonates. The Rock Creek sample exhibited more heterogeneity, both in thin section and in flow behavior, than did either of the other sandstone cores.
5. Three carbonate core samples (SAO, H1 and M1) which showed broad pore size distributions and preferential flow paths in thin section also showed flowing fractions of significantly less than one. Core WW2 did not exhibit such heterogeneity, and also showed no evidence of mixing between restricted and flowing pore fluids.
6. Dispersion coefficients were significantly higher for the carbonates than for the sandstones. Large dispersion coefficients are associated with wide pore size distributions.
7. Average mixing behavior on the scale of short laboratory cores is qualitatively consistent with observations of pore structure in thin section.
8. Care should be exercised to avoid uncritical acceptance of mathematical models as representative of flow behavior in natural porous media.

REFERENCES CITED

- Archie, G.E., 1952, Classification of Carbonate Reservoir Rocks and Petrophysical Considerations: AAPG Bull., v. 36, no. 2, pp. 278-298.
- Batycky, J.P., Maini, B.B. and Fisher, D.B., 1982, Simulation of Miscible Displacement in Full Diameter Carbonate Cores: Soc. Pet. Eng. Jour., v. 22, pp. 731-742.
- Carman, P.C., 1939, Permeability of Saturated Sands, Soils and Clays: Jour. Agri. Sci., v. 29, p. 262.
- Chatzis, I., Morrow, N. and Lim, H., 1982, Magnitude and Detailed Structure of Residual Oil Saturation: SPE/DOE # 10681; Presented at the 1982 SPE/DOE Third Joint Symposium on Enhanced Oil Recovery of the Society of Petroleum Engineers in Tulsa, Oklahoma, April 4-7, 1982.
- Choquette, P.W. and Pray, L.C., 1970, Geologic Nomenclature and Classification of Porosity in Sedimentary Carbonates: AAPG Bull., v. 54, no. 2, pp. 207-250.
- Coats, K.H. and Smith, B.D., 1964, Dead-End Pore Volume and Dispersion in Porous Media: Soc. Pet. Eng. Jour. (March), pp. 73-84.
- Cussey, R. and Friedman, G.M., 1977, Patterns of Porosity and Cement in Ooid Reservoirs in Dogger (Middle Jurassic) of France: AAPG Bull., v. 61, no. 4, pp. 511-518.
- Deans, H.A., 1963, A Mathematical Model for Dispersion in the Direction of Flow in Porous Media: Soc. Pet. Eng. Jour., v. 3, p. 49.
- Donath, F.A., Carozzi, A.V., Lester, S.F. Jr. and Rich, D.W., 1980, Oomoldic Porosity Experimentally Developed in Mississippian Oolitic Limestone: Jour. Sed. Pet., v. 50, no. 4, pp. 1249-1260.
- Enos, P. and Sawatsky, L.H., 1981, Pore Networks in Holocene Carbonate Sediments: Jour. Sed. Pet., v. 51, no. 3, pp. 961-985.
- Folk, R.L., 1962, Spectral Subdivision of Limestone Types in Classification of Carbonate Rocks - A Symposium: AAPG Memoir No. 1, p. 70.

- Folk, R.L., 1980, *Petrology of Sedimentary Rocks*: Hemphill Publishing Company, Austin, Texas, 184 p.
- Friedman, G.M., and Sanders, J.E., 1967, Origin and Occurrence of Dolostones, in Chilingar, G.V., Bissell, H.J., and Fairbridge, R.W., eds., *Carbonate Rocks, Origin, Occurrence and Classification*: Amsterdam, Elsevier Pub. Co., 471 p.
- Friedman, G.M., and Sanders, J.E., 1978, *Principles of Sedimentology*: John Wiley & Sons, Inc., New York, 792 p.
- Gardner, J.W., Orr, F.M., Jr. and Patel, P.D., 1981, The Effect of Phase Behavior on CO₂ Flood Displacement Efficiency: *Jour. Pet. Tech.*, v. 33, pp. 2067-2081.
- Grim, R.E., 1968, *Clay Mineralogy* (2nd ed.): McGraw-Hill Book Company, New York, 596 p.
- Heller, J.P., 1963, The Interpretation of Model Experiments for the Displacement of Fluids Through Porous Media: *AIChE Jour.*, v. 9, pp. 452-459.
- Longman, M.W., 1980, Carbonate Diagenetic Textures from Nearsurface Diagenetic Environments: *AAPG Bull.*, v. 64, no. 4, pp. 461-487.
- Lucia, F.J., 1983, Petrophysical Parameters Estimated From Visual Descriptions of Carbonate Rocks: A Field Classification of Carbonate Pore Space: *Jour. Pet. Tech.*, v. 35, no. 3, pp. 629-637.
- Morrow, N.R., 1979, Interplay of Capillary, Viscous and Buoyancy Forces in the Mobilization of Residual Oil: *Jour. Can. Pet. Geo.*, July-Sept., pp. 35-46.
- Murray, R.C., 1960, Origin of Porosity in Carbonate Rocks: *Jour. Sed. Pet.*, v. 30, no. 1, pp. 59-84.
- Murray, R.C., and Pray, L.C., 1965, Dolomitization and Limestone Diagenesis - An Introduction, in Pray, L.C., and Murray, R.C., eds., *Dolomitization and Limestone Diagenesis, A Symposium*: SEPM Spec. Pub. No. 13, Tulsa, Oklahoma, 180 p.
- Orr, F.M. Jr., Silva, M.K., and Lien, C.L., 1983, Equilibrium Phase Compositions of CO₂-Crude Oil Mixtures - Part 2: Comparison of Continuous Multiple Contact and Slim Tube Displacement Tests: *Soc. Pet. Eng. Jour.*, v. 23, pp. 281-291.
- Orr, F.M. Jr. and Taber, J.J., 1984, Displacement of Oil by Carbon Dioxide: Final Report to the U.S. Dept. of Energy, Report No. DOE/BC/10331-13 (March).

- Perkins, T.K. and Johnston, O.C., 1963, A Review of Diffusion and Dispersion in Porous Media: Soc. Pet. Eng. Jour. (March), p. 70.
- Pittman, E.D., 1971, Microporosity in Carbonate Rocks: AAPG Bull., v. 55, no. 10, pp. 1873-1881.
- Pittman, E.D., 1979, Porosity, Diagenesis and Productive Capability of Sandstone Reservoirs in Scholle, P.A., and Schluger, P.R., eds., Aspects of Diagenesis: SEPM Spec Pub. No. 26, 443 p.
- Powers, M.C., 1953, A New Roundness Scale for Sedimentary Particles: Jour. Sed. Pet., v. 23, pp. 117-119.
- Schmidt, V. and McDonald, D.A., 1979, The Role of Secondary Porosity in the Course of Sandstone Diagenesis in Scholle, P.A. and Schluger, P.R., eds., Aspects of Diagenesis: SEPM Spec. Pub. No. 26, pp. 175-207.
- Simon, R. and Kelsey, F.J., 1971, The Use of Capillary Tube Networks in Reservoir Performance Studies: I. Equal Viscosity Miscible Displacements: Soc. Pet. Eng. Jour., v. 11, p. 99.
- Simon, R. and Kelsey, F.J., 1972, The Use of Capillary Tube Networks in Reservoir Performance Studies: II. Effect of Homogeneity and Mobility on Miscible Displacement Efficiency: Soc. Pet. Eng. Jour., v. 12, p. 345.
- Spence, A.P. and Watkins, R.W., 1980, The Effect of Microscopic Core Heterogeneity on Miscible Flood Residual Oil Saturation: SPE # 9229, presented at the 55th Annual Fall Meeting of SPE and AIME, Dallas, September 21-24.
- Stalkup, F.I., 1970, Displacement of Oil by Solvent at High Water Saturation: Soc. Pet. Eng. Jour., v. 10, pp. 337-348.
- Taylor, G.I., 1953, Dispersion of Soluble Matter in Solvent Flowing Slowly Through a Tube: Proc., Royal Soc. 219, London, pp. 186-203.
- Wardlaw, N.C., 1976, Pore Geometry of Carbonate Rocks as Revealed by Pore Casts and Capillary Pressure: AAPG Bull., v. 60, no. 2, pp. 245-247.
- Wardlaw, N.C., 1980, The Effects of Pore Structure on Displacement Efficiency in Reservoir Rocks and in Glass Micromodels: SPE # 8843, presented at the First Joint SPE/DOE Symposium on Enhanced Oil Recovery, Tulsa, Okla., April 20-23.
- Yellig, W.F. and Baker, L.E., 1980, Factors Affecting Miscible Flooding Dispersion Coefficients: presented at the 31st Annual Technical Meeting of the Petroleum Society of CIM in Calgary, Alberta, May 25-28, 1980.

APPENDIX A

Table A.1	Summary of Core Properties
Table A.2a	Petrographic Data for Sandstone Cores
Table A.2b	Petrographic Data for Carbonate Cores
Table A.3	Identification of Clay Minerals by X-ray Diffraction

TABLE A.1 Summary of Core Properties

Core	Description	Rock Dimensions		Pore Volume cm ³	Porosity %	Air Permeability md	Experiment No.
		Diameter cm	Length cm				
B1	Berea Sandstone Outcrop	3.81	13.9	28.9	18.2	180	9
F2	Frannie Reservoir Sandstone	3.81	14.92	34.17	20.1	380	17
R1	Rock Creek Reservoir Sandstone	1.59	21.8	10.55	24.5	--	20
WW2	San Andres Dolomite, Willard Unit, Wasson Field	1.27	13.7	3.70	21.3	90	31
H1	San Andres Dolomite, Seminole	3.81	16.2	33.7	18.2	40	22
SA0	San Andres Dolomite, Outcrop	3.81	66.7	235.16	17	124	37
M1	San Andres Dolomite, Maljamar Field	1.59	31.5	5.67	9.1	6	34

TABLE A.2a Petrographic Data for Sandstone Cores

<u>Category</u>	<u>B1</u>	<u>F2</u>	<u>R1</u>
Mean Grain Size (μ)	250	180	325
Sorting (Friedman & Sanders, 1978)	Very Well	Poor	Moderate
Shape (Powers, 1953)	Subround	Subround to Subangular	Angular
Constituent Particles (100%)			
% Quartz	80	70	50
% Feldspar	5	20	10
% Mica	0	0	5
% Lithic Fragments	5	2	5
% Opaque Minerals	0	0	5
% Authigenic Clays	5	5	20
% Cement	5	3	5
Majority of Grain Contacts	Point	Line	Concavo-convex
Induration	Well	Very Poor	Poor
Classification Name (Folk, 1980)	Sublitharenite	Subarkose	Lithic Arenite

TABLE A.2b Petrographic Data for Carbonate Cores

Category	WW2	H1	SA0	M1
Constituents (100%)				
Allochems	2% Dolomitized ghost ooids	2% Dolomitized ghost ooids	95% Dolomitized ooids	1% Dolomitized ghost ooids
Cements	8% Pore-filling anhydrite	15% Pore-filling anhydrite	4% Rim dolomite	12% Pore-filling anhydrite
Crystalline matrix	88% Hypidiotopic dolomite	80% Hypidiotopic dolomite	-	85% Sucrosic dolomite
Insolubles	2%	3%	1%	2%
Mean dolomite crystal size (μ)	100	60	60	135
Stylolites ($\#/cm^2$)	0	0.3	0	0.6
Classification name (Folk, 1962)	Medium crystalline oolitic dolomite	Finely crystalline oolitic dolomite	Finely crystalline oolitic dolomite	Coarsely crystalline oolitic dolomite

TABLE A.3 Identification of Clay Minerals by X-ray Diffraction

<u>Core</u>	<u>Basal Spacings (Å)</u>	<u>Clay Mineral</u>
B1	7.16, 3.57	Kaolinite
	9.98, 4.96, 3.32	Illite
F2	9.98, 4.96, 3.32	Illite
R1	7.16, 3.57	Kaolinite
	9.98, 4.96, 3.32	Illite
	14.2	Vermiculite
WW2	-	-
H1	-	-
SAO	-	-
M1	-	-